Chem Soc Rev

RSC Publishing

TUTORIAL REVIEW

View Article Online
View Journal | View Issue

Bottom-up assembly of photonic crystals†

Cite this: *Chem. Soc. Rev.*, 2013, **42**, 2528

Georg von Freymann,‡[a] Vladimir Kitaev,‡[b] Bettina V. Lotsch‡[c] and Geoffrey A. Ozin*[d]

Received 1st August 2012

DOI: 10.1039/c2cs35309a

www.rsc.org/csr

In this tutorial review we highlight fundamental aspects of the physics underpinning the science of photonic crystals, provide insight into building-block assembly routes to the fabrication of different photonic crystal structures and compositions, discuss their properties and describe how these relate to function, and finally take a glimpse into future applications.

Published on 02 November 2012.

1. Introduction

There are many examples of colour that are not chemical in origin but rather physical in nature. By chemical we mean colour that originates from the absorption of light by a chromophore in molecular and nanoscale systems or solid-state materials. Here the colour originates from excitation of an electron between the ground and excited state of the chromophore by the incident light. In contrast, colour that is physical in nature stems from the way light is scattered and diffracted by random or periodic structures exemplified by the red and blue hues of the sky and the iridescent colours of opals, mother-of-pearl, sea-mouse whiskers, beetle scales, iridophoric squid, butterfly wings, feathers of peacocks and other birds (Fig. 1).[1]

In this tutorial review, the focus of the presentation will be mainly on the way light interacts with structures that are periodic at the scale of the wavelength of light, called photonic crystals. Historically, it was as long ago as 1887 that a one-dimensional (1D) photonic crystal was studied by Lord Rayleigh who showed the existence of high reflectivity of light over a well-defined wavelength range known as the stop-band. Known today as Bragg mirrors these 1D structures are used in optical physics for enhancing the efficiency of solar cells, improving the light extraction and colour purity of light emitting diodes, and optimizing the performance of lasers.

Fig. 1 Photograph of Anna's hummingbird (Calypte anna) showing highly iridescent gorget and crown feathers (photo by Camden Hackworth). Adapted from ref. 1 with permission from Royal Society Publishing.

Recently, photonic crystals have moved beyond 1D into the realm of more complex 2D and 3D light-scale photonic lattices and their practice, often stimulated by theory, has transitioned rapidly from mainstream science to advanced technology. There is ample evidence from published research of the last decade that the ability of photonic crystals to control photons can rival that of electronic crystals to manage electrons. This has proven to be especially true for high refractive index contrast 3D photonic crystals made of silicon that were envisioned theoretically in 1987 by Yablonovitch[2] and John[3] to develop an omni-directional photonic band gap offering complete control over the flow of light in all three spatial dimensions.

Today it has been said that "photonic crystals have been the classic underachievers: full of promise, sound in theory but poor on implementation". This criticism has mainly come from the optical physics community because of the difficulties experienced of adapting top-down semiconductor engineering

[a] *Department of Physics and Research Center OPTIMAS, University of Kaiserslautern, Erwin-Schrödinger-Straße 56, 67663 Kaiserslautern, Germany. E-mail: georg.freymann@physik.uni-kl.de; Fax: +49 631 205 5226; Tel: +49 631 205 5225*

[b] *Department of Chemistry, Wilfrid Laurier University, 75 University Avenue West, Waterloo, Ontario, N2L 3C5, Canada. E-mail: vkitaev@wlu.ca; Fax: +1 519 746 0677; Tel: +1 519 884 0710 3643*

[c] *Max Planck Institute for Solid State Research, Stuttgart, and Department of Chemistry, University of Munich (LMU), Munich, Germany. E-mail: b.lotsch@fkf.mpg.de; Fax: +49 711 689 1612; Tel: +49 711 689 1610*

[d] *Department of Chemistry, University of Toronto, Toronto, Canada. E-mail: gozin@chem.utoronto.ca; Fax: +1-416-971-201; Tel: +1-416-978-2082*

† Part of the chemistry of functional nanomaterials themed issue.

‡ These authors contributed equally to this work.

This journal is © The Royal Society of Chemistry 2013

techniques to fabricate photonic lattices with high enough structural and optical quality to enable the scale-up, manufacture, economics and delivery of photonic crystal components and modules into industry that can profit from the monetizing potential that photonic crystals foretell in markets that include solar cells, light emitting diodes, lasers, displays, sensors and optical fibres.

Observing that top-down approaches to the fabrication of photonic crystals often require complex and expensive lithographic instrumentation, deposition equipment and clean-room facilities, chemists realized there could be an easier way to make photonic crystals using bottom-up building-block assembly methods. The most popular chemical method today employs the crystallization of silica or polystyrene microspheres in the form of colloidal crystals, known as opals, and to use them as templates to replicate their structure in the form of inverse opals (see Sections 3 and 4). This procedure was first used to make silica and titania inverse opals that could display well defined stop bands.

This is more-or-less the story of how bottom-up assembly of photonic crystals began and in the tutorial presentation that follows we will describe the basic theoretical underpinnings and experimental accomplishments of the field from its roots to its branches. We will illustrate with some case histories how this knowledge has blossomed forth into one of the most scientifically vibrant areas of research with a multidisciplinary footprint that is spawning a number of spin-off companies, promising to manufacture and deliver bottom-up photonic crystal products to diverse markets from colour sensors for food and water quality control to colour-coded anti-counterfeiting security features on banknotes to full colour displays in the near future.

1.1. Colloidal photonic crystal milestones

If photonic crystals have been the classic underachiever, colloidal photonic crystals at least helped to demonstrate many of the countless promises made from theory – some fundamental ones even as ''firsts''. Prominently displaying colour from structure, the gemstone opal is well known even outside the scientific community. Looking for promising crystal structures displaying complete photonic band gaps, theorists pretty early realized that the diamond lattice is close to optimal. The underlying face-centred-cubic lattice is the thermodynamically preferred lattice of self-assembling colloidal photonic crystals. The resulting optical properties have been studied in detail early on. Unfortunately, this structure does not display any form of complete photonic band gap. This could have been the sudden death of its career as a photonic crystal material if not for the seminal paper by K. Busch and S. John[37] that demonstrated

Published on 02 November 2012.

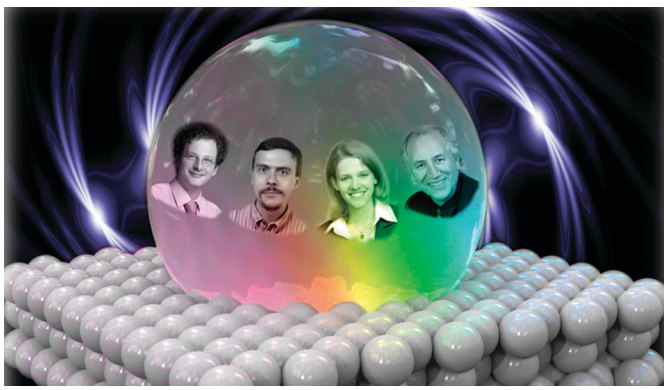

Georg von Freymann, Vladimir Kitaev, Bettina V. Lotsch and Geoffrey A. Ozin

Georg von Freymann received his PhD degree from the Physics Department, Universität Karlsruhe (TH), Karlsruhe, Germany, in 2001. He was a Postdoctoral Researcher at Institute of Nanotechnology, Forschungszentrum Karlsruhe, Karlsruhe, Germany in 2002 and at the University of Toronto, Toronto, Canada, till 2004. From 2005 to 2010 he headed a Junior Research Group in the Emmy Noether-programme of the Deutsche Forschungsgemeinschaft (DFG) at the Institute of Nanotechnology, Karlsruhe Institute of Technology, Germany. Since 2010 he is full professor for experimental/technical physics at University of Kaiserslautern, Germany. His research interests include nanofabrication technologies, photonic crystals, photonic quasicrystals and three-dimensional photonic metamaterials.

Vladimir Kitaev earned his MSc in Chemistry from Moscow State University studying cholesteric polymer liquid crystals and PhD in Chemistry from University of Toronto working with self-assembly of polymers and surfactants and rheological and tribological properties of nanoscale films. Subsequently he joined Prof. G. A. Ozin for research on monodisperse colloids, colloidal self-assembly, and photonic crystals. At present, he is an Associate Professor of Chemistry at Wilfrid Laurier University. His current research interests include ligand-protected metal clusters, size and shape control of nanoparticles, their self-assembly and optical properties, and chirality on nanoscale.

Bettina V. Lotsch studied Chemistry at the University of Munich (LMU) and the University of Oxford, and received her PhD from LMU Munich in 2006. In 2007 she joined the group of Prof. Geoffrey Ozin at the University of Toronto as a Feodor-Lynen postdoctoral fellow supported by the Alexander von Humboldt foundation. In 2009, BL was appointed associate professor at LMU Munich, and since 2011 she additionally holds a group leader position at the Max Planck Institute for Solid State Research in Stuttgart. Her research interests include ''smart'' photonic crystals, functional and hierarchically porous framework materials, as well as two-dimensional materials for energy conversion and storage.

Geoffrey Ozin studied at King's College London and Oriel College Oxford University, before completing an ICI Postdoctoral Fellowship at Southampton University. Currently he is the Tier 1 Canada Research Chair in Materials Chemistry and Nanochemistry, Distinguished University Professor at the University of Toronto, and a Founding Fellow of the Nanoscience Team at the Canadian Institute for Advanced Research. Internationally currently he is Distinguished Professor at Karlsruhe Institute of Technology (KIT). Over a four decade career he has made innovative and transformative fundamental scientific and technological advances in the field of nanochemistry, a chemistry approach to nanocrystals and nanowires, nanoporous materials, nanophotonic crystals and nanomotors that led to nanoscale constructs capable of controlling electrons, photons, phonons and motion in unprecedented ways.

Published on 02 November 2012.

the inverse structure actually possesses a complete photonic band gap, if realized in a high-index-of-refraction material like silicon. Colloidal self-assembly re-enters the stage as the most prominent templating approach for photonic crystals with a complete photonic band gap. Several firsts have been demonstrated in this system: The first complete photonic band gap at the optical telecommunication wavelength of 1.5 μm,[52] the first demonstration of enhanced and suppressed spontaneous emission,[4] the first non-linear optical experiments like all optical switching in transmittance for opals[5] and inverse opals[6] and the enhancement of third harmonic[7] and second harmonic generation.[8]

Without the need for a complete gap, several other ideas have been first implemented with colloidal photonic crystals: Graded structures for enhanced coupling efficiency,[9] binary colloidal crystal architectures,[10] porous Bragg mirrors for sensing applications,[67,69] slow photon enhanced photochemistry and photocatalysis,[11] dynamic full colour displays, enhanced light harvesting for solar-cells,[74] solid-state dye and polymer lasers,[75] increased efficiency for lithium ion battery applications[12,13] as well as applications as a dual stationary phase and detector in high-pressure liquid chromatography.[14]

In this tutorial review we will start with the underlying physical concepts behind the success of the bottom-up assembled 3D colloidal photonic crystal, how the knowhow was adapted to 2D photonic crystal architectures, expanded and enriched to include 1D photonic crystal lattices, which will be followed by a discussion of the materials and fabrication issues of these different dimensionality structures and concluded by an outlook to current and future applications.

Colloidal photonic crystals made by chemical methods may be far from perfect photonic crystals, but for a myriad of perceived and real applications even with their imperfections they are still the gold standard.

2. Basic concepts

The interaction of light with materials as well as the propagation of light within, are described by the macroscopic Maxwell's equations

$$\boldsymbol{\nabla}\cdot\boldsymbol{D} = \rho$$

$$\boldsymbol{\nabla}\cdot\boldsymbol{B} = 0$$

$$\boldsymbol{\nabla}\times\boldsymbol{E} = -\frac{\partial}{\partial t}\boldsymbol{B}$$

$$\boldsymbol{\nabla}\times\boldsymbol{H} = \frac{\partial}{\partial t}\boldsymbol{D} + \boldsymbol{j}$$

together with the constituent materials equations

$$\boldsymbol{D} = \varepsilon_0\boldsymbol{E} + \boldsymbol{P}$$

$$\boldsymbol{B} = \mu_0(\boldsymbol{H} + \boldsymbol{M})$$

Here, we use the following naming convention: $\boldsymbol{D}$ is the electric displacement, $\boldsymbol{B}$ the magnetic induction, $\boldsymbol{E}$ the electric field, $\boldsymbol{H}$ the magnetic field, ρ is the free charge density and $\boldsymbol{j}$ the free current density, P the polarization and M the magnetization.

For simplification we will assume only linear optics and isotropic materials in this tutorial so that the latter two equations reduce to

$$\boldsymbol{D} = \varepsilon_0\varepsilon\boldsymbol{E}$$

$$\boldsymbol{B} = \mu_0\mu\boldsymbol{H}$$

From this set of equations we derive the master equation describing the propagation of electric and magnetic fields. To further simplify the discussion, we will assume that there are no free charges and no free currents present in the materials under consideration, that is $\rho = 0$ and $\boldsymbol{j} = 0$. This is valid for all dielectric materials mentioned throughout this tutorial review and in the above described case of linear-optics.

2.1. Master equation and periodic structures

Combining the above equations provides us with the master equation for the propagation of the magnetic field (the equation for the electric field can be derived in an analogous fashion):

$$\frac{1}{\mu}\boldsymbol{\nabla}\times\left(\frac{1}{\varepsilon}\boldsymbol{\nabla}\times\boldsymbol{H}\right) = \frac{\omega^2}{c^2}\boldsymbol{H}$$

Here, we assumed that the magnetic field can be written in the following form:

$$\boldsymbol{H} = \boldsymbol{H}(\boldsymbol{r},t) = \boldsymbol{H}(\boldsymbol{r})\mathrm{e}^{-i\omega t}$$

For all known natural materials the magnetic permeability μ is unity at optical frequencies, reducing this equation to the following form of an eigenvalue equation:

$$\boldsymbol{\nabla}\times\left(\frac{1}{\varepsilon}\boldsymbol{\nabla}\times\boldsymbol{H}\right) = \frac{\omega^2}{c^2}\boldsymbol{H}$$

The optical properties of the photonic crystal and its dispersion relation are given by the eigenvalues on the right hand side. For homogeneous and isotropic materials (*e.g.*, a solid block of glass) the permittivity ε does not depend on the spatial coordinates and, hence, the dispersion is solely described by the materials properties alone (in this case we can move ε to the right hand side of the equation, giving us the well-known wave equation).

If we now introduce through periodic ordering a spatial dependence of the materials properties (see Fig. 2), we can control the eigenvalues and hence the optical properties of the

Fig. 2 Schematic representation of 1D, 2D and 3D photonic crystals. The electric permittivity varies along one, two or three dimensions respectively. Adapted from ref. 15.

This journal is © The Royal Society of Chemistry 2013

material through the distribution of the material: We control the operator acting on the magnetic field on the left-hand side, giving us the desired eigenvalues on the right-hand side.

Considering periodically arranged materials, *i.e.*, imposing translational symmetry into the structure,

$$\varepsilon(\boldsymbol{r}) = \varepsilon(\boldsymbol{r} + \boldsymbol{R})$$

with $\boldsymbol{R}$ being a lattice-translation vector, solutions of the master equation will have the following form, well known from solid-state physics:

$$\boldsymbol{H}(\boldsymbol{r}) = \boldsymbol{h}_k(\boldsymbol{r})\exp(i\boldsymbol{k}\boldsymbol{r})$$

with

$$\boldsymbol{h}_k(\boldsymbol{r}) = \boldsymbol{h}_k(\boldsymbol{r} + \boldsymbol{R}).$$

This solution is known as the Bloch function. This ansatz solves the master equation. As there are no analytically closed solutions, this task is usually accomplished *via* numerical methods, *e.g.*, with the plane-wave expansion method, implemented in the freely available MIT photonics band package[16]

To discuss the essential properties of periodically structured materials, we start with an intuitive approach to 1D systems, which we gradually expand to higher dimensions whenever necessary. We will end with the discussion of a full numerical calculation of the bandstructure of an inverse opal.

2.2. Photonic bandstructure, band gaps and group velocity

For the beginning we assume light propagating in a homogeneous, isotropic material with an index of refraction of n. The index of refraction and the permittivity are related *via* $n = \sqrt{\varepsilon}$. The optical properties of this material are described by the dispersion relation

$$\omega = \frac{c_0}{n}|\boldsymbol{k}|$$

with the vacuum speed of light c_0, wave vector $|\boldsymbol{k}| = k = 2\pi/\lambda$, and λ being the vacuum wavelength of light. The energy of the photons is given by $E = \hbar\omega$. Plotting the dispersion relation for forward propagation (positive k-values), results in a straight line. For backward propagation (negative k-values) we get the same dispersion properties (blue lines starting at the origin in Fig. 3).

The physics of our material will not change if we compose it in a gedanken experiment from slabs with certain thickness a, glued seamlessly together. This introduces a periodic structure with a lattice constant a. As each unit cell has absolutely the same properties as every other unit cell of our material, we can limit our discussion to just one single unit cell, the primitive cell or Wigner–Seitz cell, sufficient to construct the whole structure. The lattice vectors $\boldsymbol{R}$ in real space, in which we construct our sample and the ones of the reciprocal space ($\boldsymbol{G}$), in which we draw our dispersion relation, are closely related:

$$\boldsymbol{R}\cdot\boldsymbol{G} = m2\pi$$

m being a positive integer.

Hence, real-space periodicity results in periodicity in our dispersion relation: This leads to several branches of the

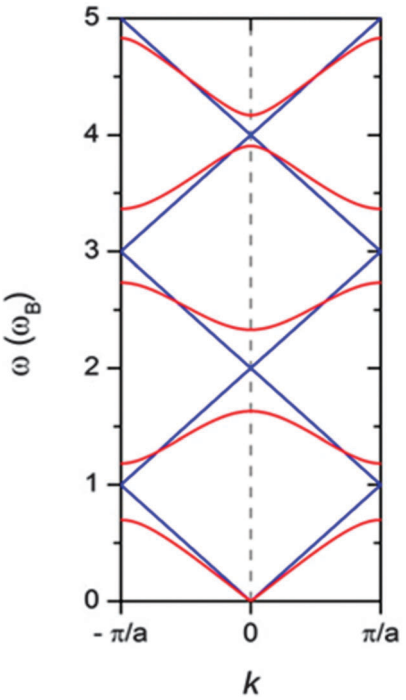

Fig. 3 Light lines and the formation of a band gap. For the calculation material slabs of thickness 200 nm and refractive indices of 1.0 and 3.5 have been assumed. The blue lines show the dispersion relation in an isotropic medium with artificial periodicity.

original dispersion relation running through our primitive unit cell in reciprocal space, called the 1st Brillouin zone, extending from $k = -\pi/a$ to $k = +\pi/a$. We also can construct the exact same picture, if we back-fold the dispersion bands starting at the origin every time they hit the boundary of the Brillouin-zone.

This leads to the picture shown in Fig. 3 with the solid blue lines. Interestingly, the crossing points of the dispersion lines of the forward and backward propagating waves are located at the frequency:

$$\omega = \frac{c_0\pi}{\sqrt{\varepsilon}a}.$$

This is nothing else but the Bragg-condition known from X-ray diffraction, but at optical wavelengths. While the concept of band structures is a very powerful one to describe materials properties, not every reader might be familiar with it. A more detailed introduction can be found in text books, *e.g.* in ref. 17.

So far, we have gained nothing but a more complicated looking description of exactly the same physics as before. Things become interesting, if we introduce different materials. Let us first assume that each slab is now divided into two materials with different permittivity, keeping the overall periodicity exactly the same.

A forward propagating wave is now partially reflected at every interface between the two materials, leading to forward and backward travelling waves at the same time. The interference of forward and backward propagating waves leads to the formation of a standing wave for frequencies fulfilling the

Published on 02 November 2012.

Published on 02 November 2012.

Bragg-condition, *i.e.*, right at the edge of the Brillouin-zone. Where will the nodes and antinodes of these standing waves be located? Due to symmetry considerations, there are just two possible solutions: The nodes and antinodes are either situated in the low-refractive index and in the high-refractive index material or the other way round. In-between-positions are forbidden, as the physics has to stay the same under sample-rotations in the laboratory. These two standing waves experience different effective refractive indices: The electric field for the standing wave with the nodes in the low-index material experiences mainly the high-index material, resulting in lower photon energy according to the above equation. The other standing wave experiences a reduced effective index and will thus be found at higher photon energies. This leads to the opening of a gap in the dispersion relation, the photonic band gap. The energetic lower band is called the "dielectric band", as its corresponding electric field is mainly concentrated in the high-index material, *e.g.*, silicon. The higher energetic band is, hence, called the "air band", as its electric field is mainly concentrated in the low index material, most of the time air. The resulting dispersion relation or band structure is depicted by the red curves in Fig. 3. For photons with energies inside the band gap, no propagation inside the photonic crystal is allowed. As can be seen directly from Fig. 3, we do not only get the fundamental band gap, but also higher order gaps, at least for one-dimensional systems. The centre position of the gap is still perfectly described by the Bragg-condition. From the above equation we directly conclude that we can shift the band gap position by either changing the lattice constant or the materials properties or both. Changing the high dielectric constant material mainly influences the dielectric band while changing the low index material mainly shifts the air band. Increasing the contrast between the two materials' dielectric functions widens the width of the band gap. In a 1D world, even the slightest index contrast leads to a full photonic band gap – this dramatically changes going to higher dimensions. Regarding the proper terminology there is some confusion in the community: We will use the term "band gap" to mark complete, *i.e.*, omnidirectional band gaps. In 1D systems every gap in the bandstructure is automatically a complete band gap. For higher dimensions, a gap might just occur for one particular direction (for opals this is *e.g.* the [111] direction) but not for others. In this case, the gap is called stop band or stop gap or even pseudo gap just to distinguish it from complete band gaps. Unfortunately, in the literature the term band gap is not clearly used and one has to check, if really a complete gap is meant.

The phase fronts of plane waves propagating through a photonic crystal experience different effective refractive indices and, hence, propagate with different phase velocities, defined as:

$$\nu_{\text{phase}} = \omega/k$$

The phase fronts in the dielectric band propagate generally at lower velocities than the ones in the air band. Much more important from an application's point of view is the velocity with which energy is transported. For absorption-free dielectric materials in allowed bands, the energy transport happens with the same velocity as the group velocity defined by the equation:

$$\nu_{\text{group}} = \partial\omega/\partial k$$

The group velocity is directly proportional to the slope of the bands. Its most remarkable property is that it vanishes at the band edges. This is perfectly consistent with the formation of standing waves, which do not transport any energy either. A direct consequence of the vanishing group velocity is an increased photon density and intensity, as well as an increased interaction time between light and matter. This property is highly interesting for amplifying non-linear effects, increasing the efficiency of photocatalysis, and enhancing light-harvesting in solar cells to name just a few applications.

If we extend our considerations to two dimensions, we will find that slow light not only can be found at band edges, but can also be found throughout the higher bands above the fundamental gap (the gap at lowest frequencies).

Let us assume for the following discussion that the two materials have again the same index of refraction, but are periodically arranged along two dimensions in a simple square-lattice. The dispersion relation is given by straight lines, which fold back at the edges of the 1st Brillouin-zone. For two dimensions this directly leads to bands with low group velocity as depicted in Fig. 4. Here, *k*-values along two different paths along the *x*-direction in two different Brillouin-zones are plotted. For the green path inside the 1st Brillouin-zone, we get the already well known dispersion relation:

$$\omega_{\Delta} = \frac{c}{\sqrt{\varepsilon}}|\boldsymbol{k}| = \frac{c}{\sqrt{\varepsilon}}\sqrt{{k_x}^2 + {k_y}^2} = \frac{c}{\sqrt{\varepsilon}}k_x$$

which is just the straight line as expected. For the blue line in the 2nd Brillouin-zone, we get:

$$\omega_{\Delta'} = \frac{c}{\sqrt{\varepsilon}}\sqrt{{k_x}^2\left(\frac{2\pi}{a}\right)^2}$$

Calculating the group velocities for both bands directly shows that group velocities for the path following the blue line

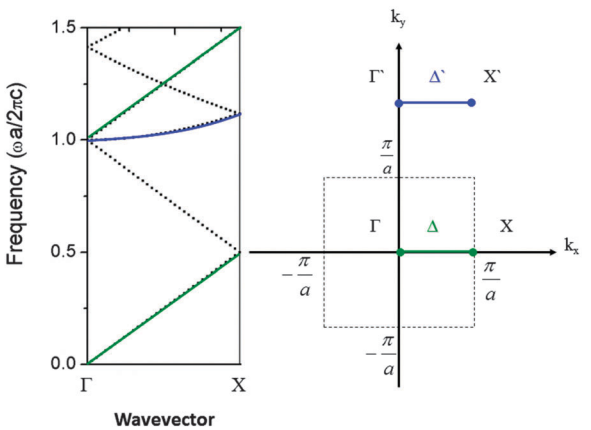

Fig. 4 The reciprocal lattice of a 2D square-lattice. A path in the 1st (green) and the 2nd Brillouin-zone (blue) are marked.

This journal is © The Royal Society of Chemistry 2013

Published on 02 November 2012.

are always smaller than the constant value of the green path and even reach zero at the centre of the Brillouin-zone (-point).

Also apparent from Fig. 4 is the fact that lattice constants vary according to the different directions along which light can propagate through the sample. For example, running along the Γ-M direction (the diagonal of the 1st Brillouin-zone) yields smaller lattice constants. From this reasoning and from $\omega = c_0\pi/\sqrt{\varepsilon}a$ follows that the spectral positions of the stop gaps along different directions differ. If a complete gap is desired, *i.e.*, an area in which no modes exist for all possible directions of propagation, the width of the gaps have to be adjusted *via* the refractive index contrast. In two-dimensional systems this can still be done for each polarization of light (transverse electric and magnetic, respectively) independently, as Maxwell's equations decouple. For 3D structures like inverse opals, this is no longer true and the full problem has to be solved. However, numerical solutions predict the opening of a complete photonic band gap for index contrast higher than 2.8, putting some restrictions onto the choice of materials for real-world realizations. Compared to the refractive index contrast of 1.9 required to open a complete band gap in a diamond lattice (*e.g.* in the famous woodpile geometry), this number is the price we have to pay to benefit from the power of self-assembly. Fortunately, all of the features discussed in our intuitive model are still present, if we take a closer look at the photonic band structure of a silicon inverse opal (see Fig. 5).

The gap discussed in our intuitive picture can be found in the Γ-L direction between bands 2 and 3, acting here as a stop band (or pseudo gap) along one propagation direction. As discussed, opening a complete band gap needs careful consideration of geometry and materials. Here, the complete photonic band gap is located throughout all propagation directions between bands 8 and 9 (blue hashed area). Flat bands with reduced group velocity as discussed for the two-dimensional model can be found in the spectral region above

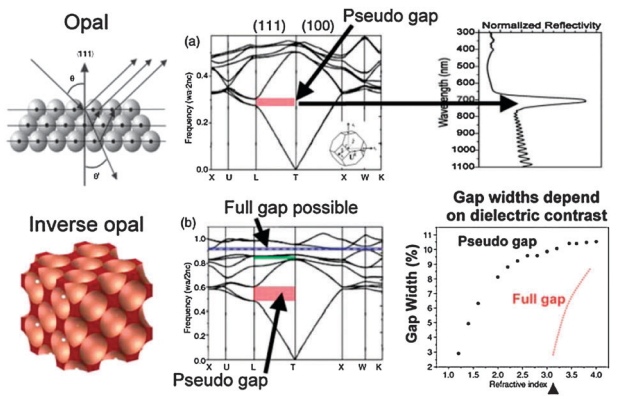

Fig. 5 Top row from left to right: Opal structure; photonic bandstructure calculation for a silica opal. The stop band is marked in red; reflectance measurement along the 111-direction. Bottom row from left to right: Inverse opal structure; photonic bandstructure calculation for a silicon inverse opal. The stop band is marked in red. The complete photonic band gap is marked in blue; Gap widths plotted over index of refraction. Reprinted by permission from John Wiley and Sons: N. Pinna and M. Knez (eds.), 1st edition, Wiley-VCH, Weinheim, 2011.[56]

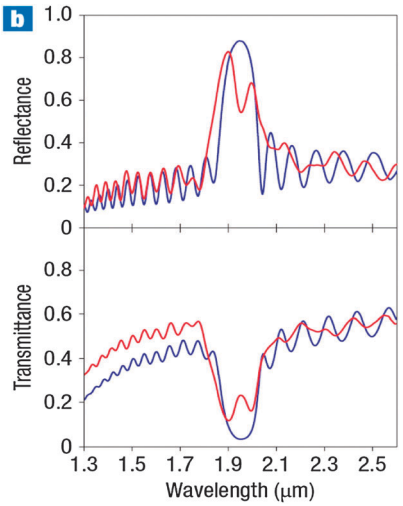

Fig. 6 Reflectance and transmittance spectra of a silicon inverse opal (blue curves). If a functional element is introduced, states inside the gap exist, leading to increased transmittance (red curves). Reprinted by permission from Macmillan Publishers Ltd: *Nature Photonics*, 2008, **2**, 52.[18]

the photonic band gap and above the stop band. Their shape is more complicated due to back-folding from higher Brillouin-zones in three-dimensions, but their behaviour is actually the same. For low photon energies, *i.e.*, for long wavelengths of light, an almost straight dispersion relation can be found, showing the effective index of refraction of the photonic crystal (bands starting from the Γ-point).

As all photonic crystal properties discussed so far and shown in the band structure are for perfectly periodic and infinitely extended structures only, the question arises how these properties show up in measurements of real, finite-sized photonic crystals. Fig. 6 shows transmission and reflection data from a silicon inverse opal where the strong transmittance dip at 1.95 μm is due to the photonic band gap. Due to the finite size, a small amount of light is still able to propagate through the sample, but is exponentially damped. The strong suppression of transmittance at higher frequencies is due to two concurrent processes: first, the slow velocity in the flat higher bands results in a high group index and, hence, to a high reflectivity of these bands. Due to the reduced speed of light, the time to interact with the surrounding sample is increased, enhancing also the efficiency of scattering processes at small imperfections of real world samples, leading to further loss of light in transmittance. Second, for higher frequencies photon wavelengths become small compared to the period of the lattice and diffraction of light occurs, leading to further loss in the forward direction, as higher diffractive orders than the always present zeroth order appear. Below the band gap a second dip in transmittance indicates the stop band along the propagation direction, not shown in Fig. 6 but discussed in Fig. 5. These features can be explained from the band structure. But what about the oscillations observed above and below the band gap? These are finite-size effects: The photonic crystal with its two surfaces acts like a Fabry–Pérot resonator, showing these characteristic resonances.

They are very helpful for optically determining the thickness of the photonic crystal slab and also allow deducing the effective index of refraction of the sample. This can be done using the following equation:

$$\frac{1}{\lambda_m} = \frac{m}{2Ln_{\text{eff}}}.$$

Here, m indicates the order of the fringe, L the sample thickness, and λ_m the wavelength of the corresponding fringe.

2.3. Analogy to semiconductors and functional elements

On first sight, the photonic band structure resembles the electronic band structure of a semiconductor. Hence, photonic band gap materials are sometimes termed ''semiconductors for light''. This analogy can be further stretched, if we consider now introducing ''defects'' into the perfect periodic structure, hence, breaking its symmetry. We have to distinguish between intrinsic defects, *e.g.*, stacking faults, missing building blocks or their variations in size, and functional defects, which are intentionally introduced and which will be solely discussed in this section. To clearly distinguish these two kinds, we will call the latter ''functional elements'', showing them due respect, as their fabrication is still extremely challenging, especially in colloidal systems.

Doping in semiconductors introduces electronic defect states located inside the electronic band gap, giving the pure semiconductor functionality, *e.g.*, allowing the construction of pn-junctions and, hence, solar cells, light emitting diodes, and semiconductor lasers. Introducing functional elements in photonic crystals accordingly creates allowed states for light propagation inside the photonic band gap. Although there are no intrinsic photons present in a photonic crystal and although we cannot excite photons from below the band gap to above the band gap like the electrons in semiconductors, these functional elements are extremely important for many of the envisioned photonic crystal applications.

Consider again a one-dimensional, infinitely extended photonic crystal, composed of high- and low-index-of-refraction materials slabs. If we separate this photonic crystal into two half-space-filling parts, photons with a frequency inside the photonic band gap impinging onto the interface will be perfectly reflected. Separating the two photonic crystal half spaces by a distance d then leads to a resonance at wavelength, $\lambda = 2d$. As the photons inside this resonator cannot escape into the photonic crystal, we find an exponential decay of the field strength into the photonic crystal, a so called evanescent tail. These zero-dimensional functional elements or resonators lead to one resonance frequency inside the photonic band gap, allowing photons to pass the photonic crystal. These elements can be made to respond to chemical and physical stimuli, which prove to be extremely useful for creating, for example, active frequency filters, sensing elements and laser cavities.

Adding a second resonator to our photonic crystal leads to a coupling between the two resonators and to a frequency-splitting of the resonance frequencies. The coupling strength and, hence, the amount of splitting, can be controlled by the distance between the two resonators. If we place in our infinitely extended 1D photonic crystal every n-th unit cell a resonator, the splitting results into infinitely many states and, hence, to the creation of a pass band inside the photonic band gap. Its dispersion relation follows cosine behaviour. This provides us with the opportunity to design the dispersion relation, *i.e.*, the position of the pass band as well as its spectral width and its group velocity.

In two- and three-dimensional structures, this coupled resonator optical waveguide can lead to a true one-dimensional waveguide, if the spacing between the resonators vanishes. Light can then be guided around wavelength-size sharp corners throughout the photonic crystal as it cannot escape into the bulk of the photonic crystals due to the photonic band gap. As an example of an experimental realization we refer to Fig. 6. The red curves show reflectance and transmittance data for a photonic crystal containing a waveguide, spectrally located inside the band gap and, hence, allowing light to propagate through the structure. This results in the prominent peak in the transmittance spectra right at the centre of the band gap.

As dispersion relations of functional defects in two- and three dimensional photonic crystals can only be computed numerically, we will limit ourselves for this tutorial review to the intuitive and qualitative discussion of functional defects given above. The following sections give deeper insight into how such materials can be realized and we will discuss experimental results with respect to our simple reasoning presented in this theoretical part.

3. Colloidal self-assembly

Photonic crystals, a material comprised of periodic arrays of sub-microscale elements, can be fabricated both by top-down and bottom-up approaches.[19] Top-down fabrication produces increasingly smaller elements using precise macroscopic tools, such as lithography with photons, electrons, atoms and ions as well as with embossing and scanning tips methodologies. The drawback of top-down fabrication is its generally serial nature that makes it progressively slower and costlier to produce smaller periodically arranged features over large areas with increasingly high precision. By comparison, bottom-up approaches involve assembly of smaller building blocks into larger area periodic structures, as commonly occurs in Nature. A combination of top-down and bottom-up fabrication strategies offers a synergy advantage, which will be outlined in a relevant context, while the major subject of this tutorial review are bottom-up approaches as they are more accessible for prototyping in research labs.[19]

As discussed above, photonic crystals are engineered to manipulate electromagnetic radiation in the wavelength range from ultraviolet to visible to near-IR (*ca.* 300 nm to 2000 nm). Consequently, PC periodicity should be on the order of a fraction of the wavelength (see part 2.2) of the band gap, which defines a size range of PC building blocks from *ca.* 50 to 1000 nm. A precision of the PC regularity (variation in size, shape and reproducibility in positioning of the repeating units)

Published on 02 November 2012.

 This journal is © The Royal Society of Chemistry 2013

needs to be better than 5% with the surface defects/irregularities not exceeding 1/10 of the operating wavelength to minimize deleterious scattering effects. Furthermore, in order to improve precision of PC building blocks, they can in turn be assembled out of smaller sub-components. These considerations define a broad range of sizes of PC building blocks from *ca.* 10 to 1000 nm. This range is appreciably larger than molecular dimensions (and that of regular structures produced by molecular self-assembly) and is the realm of colloid science.

Colloid science can be considered by several accounts as a forerunner of nanoscience. Colloidal systems, including inorganic pigments, were used by humans since the dawn of civilization. One of the first documented descriptions of colloidal systems is the series of research manuscripts of Francesco Selmi in the 1840s on colloidal sulphur, silver chloride, and Prussian Blue, which he referred to as ''pseudo-solutions''. Later in 1861 Thomas Graham introduced the term ''colloid'' (from Greek ''kolla'' (κολλα) for glue) to describe ''pseudo-solutions and to emphasize the distinctive behaviour of matter with properties intermediate between that of a solution and a suspension. Prominent work of Michael Faraday on gold colloids and colloidal stability in the 1850s made an important contribution to the field. Wolfgang Ostwald should also be acknowledged for his pivotal role in establishing the physicochemical foundations of colloid chemistry, the principles of which are expounded in his classic 1914 book ''The World of Neglected Dimensions''.

In the context of our tutorial review, colloid science deals with preparation and stability, as well as assembly of colloidal particles that can satisfy all the diverse requirements of PC building blocks. An example of a relevant colloidal system is a dispersion of solid particles in liquids that are versatile in preparation and handling. Through controlling colloidal interactions, uniform in size and shape (monodisperse), colloids can be assembled into organized arrays, so-called colloidal crystals (CCs) that share a lot of similarities with common crystalline lattices (Fig. 7). CC structures with ample structural and functional diversity can be produced. For instance, deposition of several CC layers (with different particle sizes, materials, *etc.*) can be readily accomplished. There is more flexibility with non-epitaxial deposition of CCs compared to atomic/molecular systems given that the energy mismatch of colloidal packing is rarely sufficient to drive the system to new states of rearranged layers. For the same reasons, defects in CCs can be rarely corrected after assembly. These aspects underscore an important point that colloidal forces driving self-assembly are distinct from atomic forces in many ways and that should be elaborated upon further.

3.1. Colloidal forces

Colloidal interactions and forces are incredibly multifaceted[20] as a consequence of a great diversity of colloidal systems including the materials and assembly conditions (as well as historic developments resulting in an exhaustive and often redundant rather than unifying description). Thus, for the purpose of this tutorial review it will be helpful to focus on

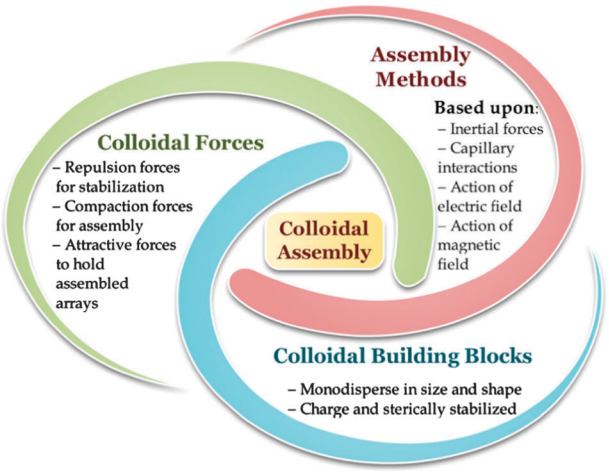

Fig. 7 Diagram of the key components of colloidal assembly.

key interactions that are crucial for colloidal assembly. In particular, three different types of forces should be considered.

First, an intrinsic driving force for ordering must be present, *e.g.* originating from entropically favourable packing of monodisperse colloids into ordered arrays. Upon colloidal ordering, free energy is gained by the enhanced collective mobility modes of particles in the arrays; in the presence of solvents, formation of concentrated colloidal phases additionally increases the degrees of freedom accessible to solvent molecules. In order to assure that formation of ordered colloidal arrays in a system is thermodynamically favourable, colloidal monodispersity (size- and shape-uniformity) is one of the key factors. An instructive illustration is the packing of uniform marbles (monodisperse macroscopic hard spheres) into hexagonal close-packed arrays, which is similarly entropically favourable.

The second factor is long-range (often macroscopic) forces that act to bring particles together. Examples of such forces responsible for colloidal compaction are gravity or centrifugal forces for sedimentation-packed colloids, compression forces for Langmuir layers, and long-range capillary forces for CC films. For the illustration of marble packing, referred previously, gravity and confinement by container walls bring the marbles together.

The third key factor (often underappreciated) is the presence of sufficient repulsion forces to overcome premature particle aggregation (sticking) due to universally acting attractive van der Waals forces and related interactions, such as favourable minimization of high surface area of colloids by aggregation. Notably, the repulsion forces responsible for preventing premature aggregation upon particle assembly are essentially the same forces/interactions that provide colloidal stability. Two primary examples of such forces are electrostatic repulsions[21] by charge stabilization in polar solvents (*e.g.* water and alcohols commonly used for assembly) and steric interactions that function more universally in all solvents. Steric repulsion is realized by solvated absorbed layers, *e.g.* of polymers that can be weakly physisorbed on a particle surface due to multiple interactions of ligands–surfactants that should have stronger

Published on 02 November 2012.

adsorption.[20] The steric repulsive force is predominantly entropic in origin. Both electrostatic and steric stabilization can be accomplished by molecules that bind strongly to colloidal surfaces and modify their interfacial properties, and thus act as ligands and surfactants. For the marble illustration, the analogy that brings repulsive interactions becomes more complex: first, the marbles naturally should not be too sticky to pack closely (otherwise they pack randomly and loosely); second, the marbles have to be gently shaken in order to access the states of optimal close packing and to provide them with the mobility naturally imparted to colloids by thermal energy of dispersion media (Brownian motion).

In the main context of this tutorial review, the primary role of electrostatic forces is to provide necessary repulsion between colloidal particles of a similar charge. At the same time, the overall role of these forces is undoubtedly more complex. Importantly, an overall colloidal system is charge-neutral with a counter-ion cloud bearing an opposite charge to that of the surface of colloidal particles. The counter-ion cloud has a complex charge distribution, which is sensitive to many factors, in particular electrolyte concentration, and plays a significant role in electrostatic interactions. Perhaps somewhat counter-intuitively, in colloidal systems of the same charge particles with long-range charged forces (low electrolyte concentrations, dialyzed dispersions) the attractive interactions between particles lead to formation of ordered arrays where particles are separated by a distance comparable to, or exceeding their size.

In colloidal binary systems with opposite particle charges, that are not yet fully explored but promising for PCs, two research directions are worth mentioning. The first one is colloidal systems with compensated van der Waals interactions by using solvents with matching refractive index, developed by the van Blaaderen group.[21] The second is the richness of structures attained by co-assembly of oppositely charged nanocrystals, which at the very least can find their application in assembly of diverse well-defined colloidal building blocks for PCs.[21]

3.2. Colloidal building blocks

The essential requirements for colloidal building blocks (CBBs) for PCs outlined above include sizes ranging from 10 to 1000 nm, and sufficient monodispersity and colloidal stability to enable thermodynamically-favourable assembly.

One of the most common and straightforward to prepare monodisperse shapes of CBBs is spherical, which is formed by amorphous materials (*e.g.* polymers, silica) and isotropic polycrystalline aggregates. Consequently, PCs assembled from spherical particles are most studied. In addition, more complex CBBs can be in turn constructed out of spherical monodisperse particles, such as regular polyhedral assemblies or concentric (core–shell) structures.[22,23] With the advancement of colloidal synthesis and assembly, PCs built out of non-spherical colloids such as ellipsoids, plates and rods are becoming an emerging research area.[22,23]

It is instructive to discuss first what properties make most successful CBBs by considering two key systems for colloidal photonic crystals: silica and latex (see Fig. 8–10 for representative SEM images of their assemblies). Silica microspheres were

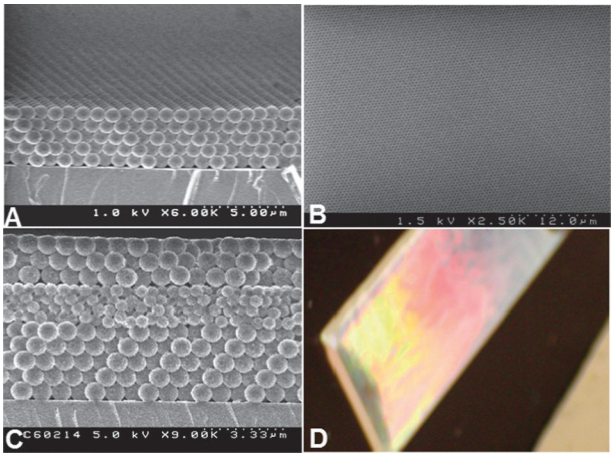

Fig. 8 Scanning electron microscopy (SEM) images (A–C) and optical photographs (D) of silica CC films assembled by IHEISA using spheres with diameters of 635 nm (A), 480 nm (B), 850 and 480 nm (C), and 850 nm (D). Images adapted from ref 31.

one of the first monodisperse inorganic colloids that have been prepared and characterized directly by imaging with electron microscopy by Stöber in 1968. This robust colloidal silica preparation utilizes hydrolysis of silicon alkoxides in a mixture of water (reactant) and alcohols (polar media) catalyzed by ammonia (that also acts as a charge stabilizer), and thus is fairly simple to prepare and amenable to scaling. Another important aspect is that silica is a nearly ideal inorganic colloidal system since it is amorphous and has a very low point of zero charge (pzc) at pH = 2 as an acidic oxide. As a result, silica particles are spherical and highly negatively charged in neutral and basic media. This makes silica colloids naturally charge-stabilized, which is generally not the case with other oxides, such as alumina, zirconia, and titania. For instance, titania can be considered as an antipode of silica. Titania pzc is controversially defined at around pH = 6, so because of dissolution issues it is difficult to stabilize electrostatically in aqueous solutions and thus to handle in colloidal assembly.

Latex is another monodisperse colloidal system that has found wide-spread applications in colloidal assembly. The original meaning of ''latex'' refers to milky (think of latte) dispersions of polymers in water. Latexes can be prepared out of most water-insoluble polymers *via* emulsion and dispersion polymerization. Most common latex polymers are polystyrene (PS) and acrylates, *e.g.* poly(methyl methacrylate) (PMMA). Both PS and PMMA have glass transition temperatures well above RT, so that their latex particles remain rigid and non-aggregating in colloidal arrays in contrast to film-forming latexes, such as those based on polyvinyl acetate, PVA. From a colloidal perspective, it should be immediately recognized that pure non-polar polymers, such as PS, are not thermodynamically stable when dispersed in water and should aggregate. In this respect, the uniqueness and advantages of colloidal latex systems are in well-developed chemical stabilization achieved through the versatile control of polymerization reactions where macromolecules (and resulting colloids) can be tailored to

Published on 02 November 2012.

 This journal is © The Royal Society of Chemistry 2013

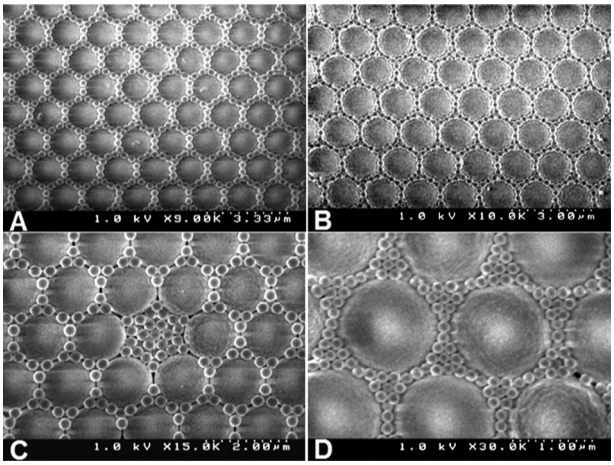

Fig. 9 SEM images of binary colloidal crystals produced by co-assembly of larger PS spheres of 1280 nm and smaller spheres: 260 nm silica (A), 225 nm PS latex (B), 280 nm silica (C), and 150 nm silica (D). Images adapted from ref. 10.

incorporate stabilizing fragments (*e.g.* charged initiators and co-monomers). As a result, the latex surface chemistry and surface potential, its colloidal stability and interactions can be conveniently modified to suit the assembly requirements. The size-control in latex systems is also well established, *e.g.* through seeded nucleation. The latex synthesis is readily scalable which provides an additional potential advantage of using exhaustive purification to further improve monodispersity of the size distribution. Polymer particles are amenable to post-modification, *e.g.* gradient etching (Fig. 10) and can serve as a convenient template, *e.g.* for inverse opals.

Since all major classes of materials can be prepared in a colloidal form, the key criteria of CBB suitability for self-assembly are the ease and practicality of achieving: (i) colloidal stabilization through charged and/or steric interactions; (ii) size (and monodispersity) control through the judicious selection of precursors and stabilizing ligands; (iii) shape (morphology) selection. In this context we will briefly describe representative examples of dielectrics, semiconductors, and metals and key aspects of their colloidal stabilization and assembly.

For semiconductors, silicon served as a material for pioneering inverse opals with a full band gap at 1500 nm. While silicon will likely remain impractical to produce sub-micron colloidal particles and CBBs, silicon nanocrystals, Si-NCs, that have been successfully developed recently, are suitable for versatile CC templating in ambient conditions.[24] An advantage of silicon colloidal stabilization is in facile formation of an oxidized surface layer of silica that is commonly utilized in Si-NCs.[25]

Inorganic oxides are among the most commonly used dielectric materials of CBBs for PCs due to their usually low light absorption in the visible and NIR and the relative ease of electrostatic stabilization in polar solvents. Two typical examples of stabilizing surfactants/ligands used for oxides are siloxanes and phosphonates. Polyvinylpyrrolidone, PVP, functions as a universal steric stabilizer in aqueous dispersions due to amide groups capable of binding to most polar surfaces (binding of an individual repeating unit is weak but overall binding energy is enhanced entropically by a zipper-like effect of a polymer chain). Among oxides, titania is commonly used in photonic crystals due to its high refractive index and photocatalytic properties. As previously mentioned, an intrinsic surface charge of titania is low compared to silica, so electrostatic stabilization is more difficult. Additionally, in direct relationship with its high refractive index, attractive van der Waals interactions are stronger for titania that makes its self-assembly challenging overall. One of the approaches to circumvent this challenge is colloidal crystal templating to form inverse opals, which will be discussed later.

Metal nanoparticles self-assembled in close-packed 2D and 3D arrays lose their plasmonic properties and become merely corrugated reflective surfaces. Thus, metallodielectric composites (where dielectric separates interacting plasmons), are needed to serve as functional PCs strongly interacting with light, where plasmon energy can be readily tuned *via* the metal part of CBBs. From the point of colloidal stabilization, the surface of commonly employed CBB metals, such as gold and silver, has to be usually modified by strongly binding ligands (*e.g.* thiols, phosphines, amines) in order to counteract aggregation.[25]

Self-assembly of anisotropic CBBs permits versatile control over the dimensionality of colloidal photonic crystals. For instance, 1D PCs can be prepared using 2D colloidal building blocks (*e.g.* large platelets of clay and other layered materials). 2D photonic crystals can be produced by assembly of periodic arrangements of 1D wires or realistically, long rods. Colloidal particles of intermediate (in this context) dimensionality, such as shorter rods or smaller platelets, can be assembled into anisotropic PCs with tailored birefringent properties. Core–shell architectures of CCBs enable realization of PCs with modulated structures. For colloidal particles composed of two or more distinct materials (Janus particles, patchy colloids) directional self-assembly can be accomplished through selective interactions. Self-assembly, based on several types of CBBs exemplified by binary colloidal crystals, offer diverse opportunities for creating periodic arrangements of CBBs (see Fig. 9). Multilayer films can be readily produced by consecutive depositions (Fig. 8C). The gradient can be imparted to CPCs through the controlled modification, such as preferential etching of top layers by air/oxygen plasma (Fig. 10).

Incorporation of chiral constituents into CPCs should enable realization of selective interactions with polarized light,

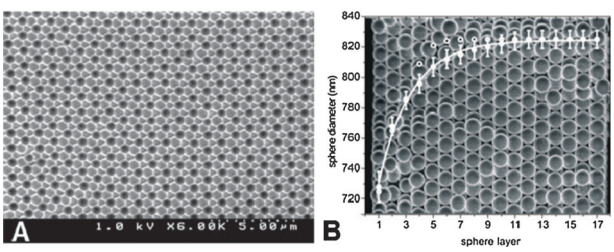

Fig. 10 SEM images of polystyrene colloidal crystal films subjected to air plasma to create gradient layers at the surface. Top view (A) and cross-section with the analysis of the sphere diameter change as a function of the depth from the surface (B). Adapted from ref. 9.

Published on 02 November 2012.

Table 1 Summary of classification of colloidal assembly methods

Assembly method	Driving force	Resulting structures	Additional factors
1. Based on gravity/inertial forces (*macroscopic forces bringing colloidal particles into close proximity/contact*)			
1.1 Sedimentation	Gravity *vs.* buoyancy	3D (Bulk)	
1.2 Centrifugation	Centrifugal due to density difference	3D (Bulk)	
1.3 Spin-coating	Centripetal	Films	Can be directed by substrate patterning; may have capillary contributions
1.4 Langmuir–Blodgett films	Compression forces of a moving barrier	Thin films and monolayers	Interfacial forces
1.5 Shear ordering	Shear flow, shear forces	Thin films	Directed by substrate confinement; may have capillary contributions
2. Based on capillary forces (*driven by surface tension of evaporating solvent*)			
2.1 EISA	Capillary	Films	
2.2 Dip-coating	Capillary	Films	Fast withdrawal rates lead to thinner layers and more defects
2.3 Aerosol spraying	Capillary	Films, droplets	Often droplet confinement
2.4 Assembly at liquid–liquid interfaces	Surface tension and capillary forces	Thin films and monolayers	Several mechanisms depending on compatibility of liquids and colloids
3. Based on interactions of colloids with electric field			
3.1 Electro-phoretic assembly	Action of electric field on charged particles	Thin films or patterns in between electrodes	Electrochemical interference
3.2 Dielectro-phoretic assembly	Action of non-uniform electric field on dielectric materials	Defined by the applied field	Commonly by ac field
3.3 Optical tweezers	Action of non-uniform light intensities on dielectric materials	Defined by light intensity gradients	Use of laser irradiation, *e.g.* interference patterns
3.4 Electro-osmotic assembly	Action of electric field on ionic cloud of colloidal particles	Layers at electrodes	Important for organization and reorganization at electrodes surfaces
4. Induced by magnetic field	Action of magnetic field on ferro- and paramagnetic particles	Diverse structures can be readily attained	Requires ferromagnetic or paramagnetic materials
5. Multifactor assembly, *e.g.* microfluidics	Shear upon flow and capillary upon liquid removal	Micro-confined assemblies	Directed by confinement conditions

Published on 02 November 2012.

which is advantageous for biosensors based on circular dichroism and metamaterials. Assembly of chiral CBBs should, in principle, lead to formation of supramolecular structures similar to cholesteric liquid crystals.[26] One of the possible routes to realization of chirality in CBBs is imprinting with chiral ligands. For instance, intrinsically non-chiral colloids, such as nanoprisms, stabilized with chiral ligands were shown to assemble into helical columnar colloidal crystals resembling chiral liquid crystal mesophases.[27] Given intrinsic chirality of clusters stabilized with chiral ligands,[25] their supramolecular assembly into colloidal particles with preservation of chirality can be envisaged. Another relevant system concerns helical supramolecular self-assembled structures templated by inorganic materials, such as silica, for creation of chiral CBBs.[26]

Colloidal building blocks offer advantageous opportunities of tuneable refractive indices for PCs with sensing capabilities. The materials for such CBBs are metal oxides, zeolites, mesoporous materials, clays, MOFs, ZIFs and related systems templated with amphiphilic surfactants and block-copolymers. PCs with the hierarchy of porosity from intercrystalline to mesoscopic colloidal interstices have been successfully demonstrated.[22]

3.3. Colloidal assembly

First, it should be reiterated that CBBs for assembly are required to be sufficiently monodisperse and appropriately stabilized so that their entropically favourable packing can be realized. Practically speaking, the quality of CBBs frequently becomes a crucial limiting factor in assembly. With suitable CBBs, the central objective of colloidal assembly methods is to provide the driving force to bring particles together in a uniform organized fashion for formation of high structural and optical quality colloidal crystals. Accordingly, assembly methods can be classified primarily based on the driving force of colloidal compaction, namely, gravitational/inertial, capillary (and surface tension), electric and magnetic fields (see Table 1). Another classification criterion is the dimensional aspect of the formed colloidal crystals in a continuum from 3D bulk crystals to thick films and to 2D monolayers. (1-D structures can also be realized through substrate templating.) Other relevant characteristics of self-assembly methods[22,23] including an effect of confinement (directed self-assembly), use of multiple building blocks, and hierarchy of co-assembly.

In the classification context, we can briefly address a subtle distinction between ''colloidal self-assembly'' and ''colloidal assembly''. The former is the case when ordering forces originate and act on a molecular/colloidal length-scale. In the case of involvement of external forces (*e.g.* centrifugation), the use of ''colloidal assembly'' may be more appropriate, although for the purpose of this tutorial review, these terms can still be used interchangeably. Most assembly processes involve application of some external influence (forces or changes in system conditions).[28] At the same time, colloidal assembly (*i.e.* ordering of particles in organized arrays) occurs without human intervention[29] (at least without the direct ability to influence positioning of individual particles driven by colloidal interactions) and thus satisfies a broader definition of ''self-assembly''.[20,29]

Among the forces bringing colloidal particles together, sedimentation is one of the more straightforward. Colloidal particles can be compacted by sedimentation when particle density is appreciably different from that of a dispersion

 This journal is © The Royal Society of Chemistry 2013

medium. Commonly, CBBs have larger densities that result in gravitational forces exceeding buoyancy forces. Brownian motion, is a significant factor for packing and assembling smaller particles that brings a practical size limit for sedimentation assembly to *ca.* 100 nm for silica and *ca.* 200 nm for latex in aqueous dispersions. The colloidal compaction through density difference can be accomplished more effectively by centrifugation. Centrifugation makes compaction feasible for most particle sizes provided sufficiently strong centrifugal forces are applied (even a small density difference, such as between PS latex (1.05–1.06 g cm^{-3}) and water (0.99–1.00 g cm^{-3}) can be sufficient for compaction). Colloidal assembly driven both by centrifugation and sedimentation can be further enhanced by confinement, *e.g.* using epitaxially patterned substrates or surface relief patterns. Still, the main restriction of these methods is the limited control over CC formation, such as CC thickness and, more generally, integration into devices.

In spin-coating, centripetal forces are responsible for spreading of a uniform film of a colloidal dispersion on a substrate and together with gravitational forces, particle compaction. For the formation of thicker uniform films, higher viscosities are desirable, so either more concentrated dispersions or polymer additives can be used. During solvent evaporation from spin-coated films, capillary forces are also a contributing factor to colloidal assembly and final stages of particle ordering. The advantage of spin-coaling is a demonstrated ability to prepare large-area uniform films and compatibility with established technological processes.[30]

In formation of Langmuir Blodgett (LB) films, a layer of colloidal dispersion is deposited on a surface of a non-miscible less-volatile solvent.[22] Then after or during evaporation of the dispersion solvent, particles are compressed by a moving barrier of the trough, which exerts a compaction force. Compared to LB films of amphiphiles, higher densities of the inorganic colloids can result in particles sinking from the top layer, which presents appreciable practical limitations. While LB deposition is most suited for preparation of large-area monolayers, transfer of the ordered colloidal layers from the liquid interface to the substrate is prone to disruptions that largely limit colloidal LB films to scientific studies.

Upon ordering of colloidal dispersions by shear flow, the action of shear (lateral) forces is more complex; effects of confinement and the surface properties of the substrate are inherent due to particles sheared in between two surfaces. In most of the cases, assuring uniformity of the shear forces can be challenging, so this method is largely limited to research studies. At the same time, shear ordering by flow is an important component of lab-on-a-chip CPCs assemblies.

Capillary forces act on interfaces between colloidal particles and solvent with other media (*e.g.* air and another solvent). Effectively, the dispersion solvent minimizes its surface area by remaining in interparticle spaces and consequently bringing the particles closer upon solvent evaporation. Arising from surface tension, capillary interactions are long-range (micron-to-mm scale), which makes them a powerful driving force in colloidal self-assembly.[28] The key parameters to manage in colloidal assembly driven by capillary forces are dispersion transport to the assembly site and uniform solvent evaporation. Upon evaporation of a dispersion droplet on a flat surface, a coffee ring pattern is commonly produced (most evaporation and deposition occurs at the outer boundary of the droplet). Thus, preparation of donut-like and dimple-shape morphologies can be achieved by dispersion evaporation in droplets, such as aerosol spraying. Uniform drying of dispersion droplets is possible when the gravity forces can be excluded (*e.g.* in non-miscible solvents of equal density) resulting in formation of ordered spherical colloidal assemblies that can be accomplished by microfluidics.

Spreading dispersion layers uniformly in order to keep constant the thickness of CC films requires different approaches. One of the simple and instructive methods is dip-coating of a planar wettable substrate. In dip coating, the substrate is withdrawn from the dispersion at a controllable uniform speed. The dispersion solvent leaves the substrate surface uniformly so that a smooth colloidal film can be formed upon drying of a dispersion layer. The main limitation of dip coating is the formation of thin CC films at typical deposition speeds (few mm per minute). In order to attain thicker films, highly concentrated dispersions have to be used that may not be always possible and practical. To improve this aspect, a closely related EISA, evaporation-induced self-assembly, in vertical films was developed. In EISA, a volatile dispersion solvent (originally and most commonly, ethanol) is evaporated slowly, on the order of cm per day, leaving a drying colloidal film in the meniscus.[22,30] The only major limitation of EISA is sedimentation of inorganic colloids during slow evaporation, especially of larger heavier particles, which results in particle departure from the meniscus and cessation of the film formation. To overcome this limitation, acceleration of the evaporation by application of either low pressures or high temperatures can be used[10,31] (see Fig. 7 and 8). In accelerated solvent evaporation, convection processes often play an important role in the dispersion mass transport and thus film uniformity, so they should be carefully taken into consideration in an optimal design of the deposition set-up.

Another related method is colloidal assembly at liquid–liquid interfaces. The key feature of this approach is the use of two solvents that should be sufficiently immiscible to form the boundary, at which colloidal ordering can be driven by interfacial energies and capillary forces.[22] Compared to EISA, this approach is more complex due to potential diversity of solvents, *e.g.* their mutual solubility, evaporation rates, and compatibility with dispersions. As a result, this method can be employed in research settings for the deposition of specific colloidal systems, especially dispersions in non-polar solvents.

Electrostatic forces play a diverse role in colloidal assembly.[21] Long-range electrostatic interactions can serve as a primary driving force of CC formation. These interactions are dominant for highly-charged colloids when the charge screening is minimized at low ionic strength *e.g.* for exhaustively deionised aqueous dispersions of latex. The formation of ordered arrays in such systems is driven by electrostatic attraction between the ionic charge clouds and oppositely charged

Published on 02 November 2012.

surfaces of the colloids. In the resulting assembly, particles are separated by a relatively large distance (comparable with the particle size), where repulsion of the same charge cores starts to balance long-range attraction. Such colloidal arrays display photonic crystal properties but are less suitable for optical devices due to their fluid nature and low modulation of refractive index; they are more practical for sensing.[32]

An electric field can be readily applied to colloidal dispersions using conductive electrodes. We can concisely outline three major processes arising from the action of an electric field on colloidal particles: electrophoresis, dielectrophoresis, and electroosmosis.[33] In electrophoresis, colloidal particles are displaced in an electric field to an opposite electrode proportionally to their surface charge. Electrophoresis is used for particle positioning, separation, measurements of surface charges, and microfluidics.[33] In dielectrophoresis, colloidal particles move as result of "forces produced by an inhomogeneous electric field," as defined by Pohl. Inhomogeneous fields are more challenging to apply but they act universally on all particles, so dielectrophoresis is becoming more actively explored and applied in particle purification, assembly, microfluidics, *etc.*[33] Dielectrophoresis by light is utilized in optical tweezers. For colloidal assembly by optical tweezers, scattering in close-packed arrays and rapidly changing optical properties of the assembled layers upon particle packing and solvent removal present a significant challenge. Electroosmosis is the electrolyte motion along charged surfaces (of colloids in this case) induced by an electric field. Electroosmosis has been shown to be important in colloidal organization in an electric field.[33] One of the limitations of colloidal assembly using an electric field is the interference of electrochemical reactions at electrode surfaces. This interference can be minimized in dielectrophoresis since an ac voltage can be used.

Magnetic fields provide a versatile driving force that can be modulated spatially, in time, and in magnitude, both for colloidal self-assembly and practical realization of tunable photonic crystals for magnetic colloids.[32] Magnetic materials are not common and preparation of their large uniform particles often by assembly of smaller ones, is quite challenging. At the same time colloidal particles, such as latex, can be doped with superparamagnetic nanoparticles. Excellent in-depth information on magnetic particles and their assembly can be found in a recent review.[34]

Finally, we briefly reflect upon two main challenges facing colloidal crystals: (i) random stacking of hexagonal close-packed planes upon colloidal organization and (ii) development of cracks upon solvent evaporation from assembling dispersions.

In assembly of colloidal arrays driven by capillary forces, the energy difference between fcc and hcp arrays and mixed close-packed lattices with the random stacking of (111) planes is minimal. All of these closed packed lattices satisfy the requirement of maximum particle contact upon solvent evaporation. As a result, random stacking can be often observed, especially in thin CC films.[35] An effective solution to overcome this problem is to use substrates with {100} epitaxy where packing of (111) planes is directed toward fcc.[22]

Cracking is common for highly ordered colloidal arrays assembled from colloidal dispersions. The origin of cracking is in a solvation layer of stable colloidal particles (either at charged surfaces or sterically stabilizing polymer layers). The thickness of the solvation layer is on the order of 1–10 nm. Upon formation of colloidal arrays by solvated particles, subsequent complete drying causes the arrays to experience shrinkage resulting in cracks. A good approach to counteract cracking is to fill the interparticle gaps either by co-assembly with smaller colloidal particles or, best, adding small controlled amount of reactive precursors upon during assembly, *e.g.* silicon orthosilicates for dispersions with aqueous solvation layers.[36] Upon reaction with water, a reactive precursor effectively replaces it with the reaction product (silicates in case of orthosilicates) that further cements the array. This approach seems also to be helpful in directing colloidal growth toward fcc arrays (without stacking faults) by changing predominant growth direction.[36]

Overall, colloids offer great versatility as building blocks for bottom-up fabrication of diverse ordered periodic structures, the main focus of which in this tutorial review are CPCs.

4. Materials and fabrication

In the early 90s, the prediction of a host of exciting photonic effects in periodic dielectrics greatly accelerated the fabrication of micro- and nanostructures with topologies, symmetries, compositions and dielectric constants allowing for the judicious manipulation of photons. However, early PC architectures were inherently micron scale owing to the intrinsic limitations of the top-down patterning techniques at hand, including layer-by-layer micromachining and etching, lithographic or holographic interference schemes. These techniques requiring elaborate sequences of drilling and deposition, alignment and etching steps, as the archetypical "Yablonovite" or "Woodpile" lattices, mainly operated at microwave or millimetre length scales. Besides the complex and time-consuming microfabrication schemes, the size of such structures has been limited to less than ten unit cells in thickness, thus making them quasi two-dimensional. Moreover, it was recognized early on that photonic band gap (PBG) materials are likely to have their largest impact at optical or near-IR wavelengths, embodied for instance by waveguides operating at telecommunication wavelengths, low-threshold microlasers, ultra-coherent light emitting diodes, sub-picosecond optical switches or all-optical transistors.[37] Therefore, the resurrection of bottom-up self-assembling structures formed from periodic arrays of submicron scale particles in essentially one single step and at low cost, at the same time giving rise to macroscopic sample sizes in all three spatial dimensions, may be considered one of the important hallmarks of PC design and has pushed the boundary of PC fabrication ever since.

As discussed earlier, an opal replica composed of a suitable high RI material, featuring a *fcc* lattice of air spheres, should possess a full PBG between the eighth and ninth bands of its photonic band structure.[38] Such ordered structures – christened inverse opals (IOs) – with high porosities and specific lattice topologies relying on interconnected air-holes can be obtained by colloidal crystal templating, *i.e.* the inversion of CCs by a sequence of infiltration and template removal steps. On the theoretical side, Bush and John expanded the portfolio of self-assembled opal-like structures with an expected full

Published on 02 November 2012.

 This journal is © The Royal Society of Chemistry 2013

band gap or pseudo gap in the near-infrared regime.[37] According to their calculations, full band gaps for both close-packed *fcc* and *hcp* structures of air spheres are expected at roughly the same frequency for materials with a RI contrast of greater than 2.8. While this obviously imposes severe limitations on the choice of materials allowing for a full PBG, the size of the band gap significantly depends on the optimal volume filling fraction, and hence the band gap may be tuned to a large extent by the preparative finesse of the experimentalist: Controlled infiltration of the artificial opal or sinter-induced necking of the spheres of the opal prior to infiltration and template removal, both resulting in controlled filling fractions of the high dielectric and so-formed intricate interconnected network topologies, provide control of the gap size.

As the requirement for an omnidirectional PBG for various applications is allayed, PCs with periodicities along two or only one dimension enter the stage, which may oftentimes be prepared more easily or offer complementary features not found in 3D PCs.

In the following, we will discuss the most prominent fabrication strategies of bottom-up self-assembled PCs with a special focus on 3D inverse opal structures, and later on expand these approaches to 2D and 1D photonic structures. However, we will start with a brief overview of the portfolio of materials that have been fashioned into PCs, to give a flavour of the kaleidoscope of properties accessible by interfacing materials chemistry, nanochemistry and photonics.

Published on 02 November 2012.

4.1. 3D photonic crystals: materials

Inverse opals (IO) have developed into the archetype PC architectures that can be routinely obtained by spontaneous or directed bottom-up self-assembly based on a diverse range of materials. In principle, IOs provide high enough porosity as well as suitable lattice topology and symmetry to exhibit a full PBG in the visible regime, given the conditions of high RI contrast and minimal absorption at the desired wavelength range (absorption coefficient <1 cm^{-1}) are fulfilled.[39] These criteria pose a substantial challenge on the material selection, thus rendering certain photonic materials suitable only for a specific wavelength range. This constraint becomes immediately evident for metals, which exhibit high absorbance in the visible range constituting a major optical loss mechanism in such structures at optical frequencies. Notwithstanding this limitation, metallic 3D structures may be quite useful for the manipulation of electromagnetic radiation at much longer wavelengths, such as microwave frequencies, yet the required structures fall outside the range of those readily amenable to chemical self-assembly. In view of the inherent limitations of metallic PCs, a range of metal IOs have been fabricated and primarily used as scaffolds with controlled porosity to study the impact of the 3D nanostructure on phenomena associated with the innate electronic and magnetic properties of metals, such as ferromagnetism and superconductivity. Nevertheless, a handful of metallic IOs have been characterized with respect to their optical properties, showing angle-dependent diffraction of light in a fashion similar to 2D surface gratings and proven useful as electrodes in electrocatalysis.[40–43]

Using a ''best of both worlds'' approach, metallo-dielectric structures composed of metal nanoparticles or ''islands'' diluted within a dielectric have recently entered the focus as possible hybrid structures that can be imbued with interesting photonic properties,[44] which may be amplified by coupling photonic and plasmonic modes in metals such as gold, silver or copper. Moreover, for an *fcc* arrangement of spheres exhibiting Drude-like behaviour of the dielectric function, for example silver, large omnidirectional and at the same time tunable PBGs have been proposed.[45] Meanwhile, this principle has been extended to metal-coated dielectric spheres in arbitrary periodic arrangements as well as to capacitive metallodielectrics potentially producing an ultra-wide photonic band gap.[46]

The potential for semiconductors as constituent materials of photonic devices is promising, especially at the interface between electron and photon management technologies, such as in solid-state lasers or high-efficiency light emitting diodes. It is the combination of electrically driven gain elements with nanostructured photonic devices that will allow for the design of a new generation of optoelectronic devices with superior performance and light control.[47]

With the utility of PCs being strongly coupled to transparency, the use of semiconductors in photonic devices is limited to wavelengths above their absorption edge. For example, one can expect near-IR photonic behaviour for a range of intrinsic or extrinsic semiconductors with fairly small band gaps such as GaAs, InP, InAs and Si, rendering them good candidates for optical telecommunication technologies operating at wavelengths around 1.5 μm.

On the other hand, wide band gap semiconductors such as GaP, Se, SnS_2, Sb_2S_3 or CdSe are particularly suitable for PCs operating in the visible. GaP, for example, fulfils both requirements for a full PBG, namely a high RI (3.42 at 560 nm) and transparency at optical wavelengths above its absorption edge (>550 nm).[39] Depending on their specific electronic fingerprint, semiconductors are well positioned at the cross section between integrated electronics and photonics, offering ample possibilities for electron to photon conversion and photon management at the same time.

The other class of materials that has been fashioned into various photonic nanostructures are dielectrics, most prominently metal oxides, but also element wide-band gap semiconductors and insulators such as diamond. The very material from which the eponymous natural gemstone opal is derived, SiO_2, has likewise been at the heart of many ''model'' artificial IOs. The lossless character and hence transparency at optical and longer wavelengths of most dielectrics as well as their chemical versatility and synthetic accessibility ideally qualify them for photonic applications, however at the expense of only moderate, if not low RIs not allowing for a complete PBG to be attained. The number of IOs made from dielectrics is vast; almost any chemically and technically relevant material has been fashioned into IOs with or without sizeable photonic properties. The scope of dielectric IOs comprises various transition metal oxides such as TiO_2, Al_2O_3,

In_2O_3 (doped and undoped), V_2O_5, WO_3, ZrO_2, ZnO, SnO_2, CeO_2, yttrium iron garnet (YIG), $BaTiO_3$ and many more.[48] In addition, "soft" dielectrics including polymers and polyelectrolytes such as PS, PMMA, various hydrogels, poly(ferrocenylsilanes) and others have been fashioned into flexible, stimuli-responsive IOs that are nowadays finding their ways into various applications such as sensing, tunable colour displays and anti-counterfeit devices.

As we have seen above, the materials used in IOs are manifold, and so is the scope of synthetic methods available to produce such nanostructures. In the following, we will discuss the most widely used and broadly applicable fabrication procedures for IOs based on selected sample materials that we believe are representative of a wide range of related materials for which similar fabrication strategies hold.

4.2. 3D photonic crystals: fabrication

The fabrication strategies for IOs are basically centred on one common motif, namely the inversion of a self-assembled CC template using the material of choice. The most important CC building blocks and CC assembly processes have been discussed in detail above; suffice it to say at this point that almost all IOs are derived from three types of CC building blocks with variable sizes, namely SiO_2, PS, and PMMA spheres, or derivatives thereof, *e.g.* spheres composed of the block copolymer poly(styrene-methyl methacrylate-acrylic acid). These building blocks lend themselves particularly well for IO fabrication, as (i) they can be obtained in different sizes in a most reproducible fashion, (ii) with a highly monodisperse size distribution and (iii) the synthesis can be operated at large scales.

The general fabrication scheme for IOs can be summarized in four steps: (1) Opal formation, (2) infiltration, (3) conversion, (4) inversion.

Infiltration proceeds by infilling the pores of the opal, typically by capillary action, with a fluid (liquid, vapour) that is subsequently consolidated by physical or chemical conversion. The nature of step (3) depends on the target material and the type of precursor used, as well as the specific fabrication procedure. For example, chemical conversion into the target polymer or inorganic solid induced by heating or reactive deposition (in contrast to physical consolidation without chemical transformation) may become necessary if a monomeric precursor is used in the infiltration step. Upon infiltration, small windows are created between the air spheres as a result of "necking" between the colloidal building blocks. These additional voids serve as channels for material transport out of the opal structure upon template removal and therefore not only affect the optical properties of the resulting IO, but ensure the feasibility of the inversion process. However, care should be taken that the necks between the template spheres are not too large through prolonged annealing or sintering, as this will prohibit infiltration by blocking the passages between the tetrahedral and octahedral interstices in the template.

The inversion procedure for the composite material is predetermined by the choice of the initial opal template and can either be chemical etching, calcination or solvent extraction. For SiO_2 templates, wet chemical etching with aqueous or non-aqueous HF or NH_4F, or strongly basic etchants such as concentrated KOH solution is used, with the fluoride based etchants being specific for SiO_2 and typically allow for a better control of the etching process. Polymeric templates are more easily removed either thermally by calcination at temperatures above $\approx$ 300 °C, or chemically by solvent extraction using *e.g.* toluene or chloroform, or by air/oxygen plasma treatment.

Although many initial synthetic difficulties, such as complete and homogeneous infiltration of the interstitials, have largely been mastered, some experimental challenges still remain: Firstly, the fabrication of single-domain colloidal crystal templates has not yet been achieved and, subsequently, the uniform deposition and growth of "single crystal"-like monolithic domains of the infilling material throughout the entire IO has so far remained elusive. Secondly, template removal needs to be done with as little disruption of the skeleton of the infiltrated material as possible. Etching, calcination and extraction may modify or even disrupt the highly porous architecture that is being formed, and therefore special care has to be taken to leave the connectivity of the replica structure intact and avoid volume shrinkage and cracking. Another challenge arises if the dielectric constant of the infilling material needs to be adjusted – oftentimes increased – through the final pore wall composition and texture.

Therefore, many of the reported protocols for IO fabrication need to be gauged by their ability to furnish homogeneous, defect-free, monolithic or even single-crystalline morphologies with crack-free and compositionally controlled pore walls. The perfect IO remains one of the holy grails in the field!

Three major protocols for IO fabrication from CC templates have been reported to date, which are distinguishable largely by the nature of the second step (infiltration), namely impregnation, gas-phase infiltration, and electrochemical deposition. Regardless of the details of the fabrication process, a prerequisite requirement in all CC templating protocols for IO fabrication is the tailoring of the precursor-to-solid transformation taking place in the interstitials of the CC template, as will be discussed in the following section.

4.2.1. Impregnation. This method relies on the infiltration of an opal template with the material of choice, or one of its precursors, followed by chemical conversion of the precursor and subsequent inversion of the composite structure. Especially for oxide dielectrics this method has proven invaluable to obtain a wide variety of compositions, the most prominent being TiO_2. Impregnation typically utilizes conversion of a precursor to form the desired composition *in situ* by a chemical reaction. Depending on the precursors used, subcategories of the impregnation method include (i) sol–gel, (ii) salt precipitation, (iii) nanocrystal sintering and (iv) gas phase protocols. These methods have been developed and refined for precursors with different reactivity and polymerization behaviour resulting in variable wall morphologies and different degrees of volume shrinkage and crack formation upon inversion.

TiO_2 is an important wide-band gap semiconductor being transparent at optical wavelengths and at the same time having a high RI of $\approx$ 2.9 for the rutile and $\approx$ 2.5 for the anatase

Published on 02 November 2012.

 This journal is © The Royal Society of Chemistry 2013

modification. Many attempts have been made to fabricate strongly diffracting TiO_2 IOs with close-to-complete band gaps in the visible, however a full PGB in TiO_2 IOs is still elusive. Initial attempts to prepare TiO_2 IOs exclusively utilized the sol–gel route based on alcoholic titanium alkoxide precursor solutions. Vos and co-workers reported on the first IO derived by multiple rounds of liquid-phase impregnation of a PS CC with a precursor solution of tetrapropyl orthotitanate in ethanol.[49] After each infiltration step, the alkoxide was allowed to hydrolyse, condense and dry in a classical sol–gel process, forming an extended and interconnected network of hydrated amorphous TiO_2 within the interstitials of the PS CC. After template removal and crystallization by calcination at 450 °C photonic bandwidths along the [111] direction of 13% were observed, corresponding to a RI of around 2.5. However, filling fractions of TiO_2 were only between 12 and 20% and the lattice parameters of the IO, being about 33% less than that of the original template, indicated significant polymerization induced shrinkage and therefore cracking of the structure. An elegant method to avoid significant volume shrinkage and at the same time ensure a high RI of TiO_2 has been reported by Colvin *et al.*[50] By annealing a silica instead of polymeric CC impregnated with TiO_2 sol at temperatures up to 1025 °C, more complete crystallization of the amorphous TiO_2 and concomitant densification was induced and at the same time shrinkage was minimized, such that after base selective extraction of the silica rather than the titania it was possible to obtain strongly diffracting IO films with a RI of anatase TiO_2 around 2.85.

The sol–gel route allows one to synthesize a wide range of transition metal oxide IOs in high oxidation states; however for many low-valence transition metal oxides as well as alkaline earth metal oxides the alkoxide precursors tend to be too reactive, thus polymerizing too fast to homogeneously infiltrate the voids of the template.

Stein and co-workers have developed an alternative route, dubbed salt precipitation/chemical conversion, which can fill the gap and provide a range of late transition metal and alkaline earth oxide IOs.[51] In a typical procedure, a PS template is impregnated with a metal salt – mainly acetates or nitrates – dissolved in ethanol or acetic acid. Subsequently, the metal salt/PS composite is impregnated with oxalic acid, leading to the precipitation of the respective insoluble, non-melting metal oxalates. Chemical conversion into the macroporous metal oxides is induced by calcination above 300 °C, which proceeds under liberation of CO and CO_2 (Fig. 11). A number of metal oxides with adjustable wall thicknesses and a high degree of structural order has been prepared following this route, including NiO, Co_3O_4, Mn_2O_3, Fe_2O_3, Cr_2O_3, ZnO, MgO, as well as $CaCO_3$, where the latter could be dubbed photonic chalk!

Nanocrystal sintering is yet another procedure that allows for tuning the ''compactness'' of the CC scaffold and hence its optical properties. The key point is to use pre-formed nanocrystals for building up the IO architecture, which at the same time is dense and less reactive than monomeric precursors, thus significantly reducing the distortion of the optical lattice by chemical transformations. One of the first examples of the

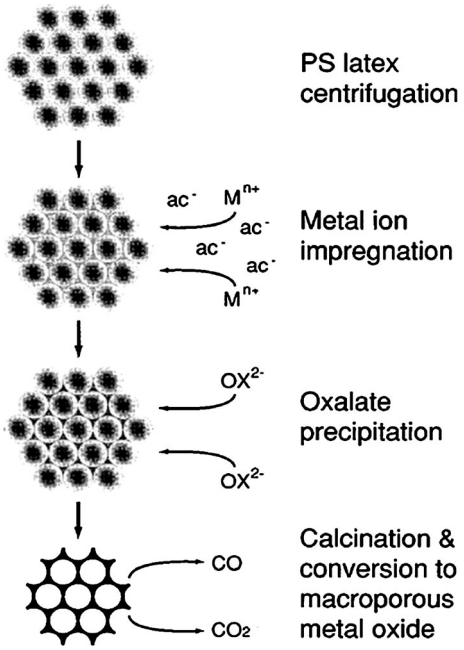

Fig. 11 Fabrication procedure of inverse opal structures of metal oxides and carbonates by the salt precipitation/chemical conversion route. Calcination transforms the metal oxalate into the respective oxide under CO and CO_2 evolution. Reprinted with permission from *Chem. Mater.*, 2000, **12**, 1134. Copyright 2000, American Chemical Society.[51]

nanocrystal sintering route has been reported in 1999 by Norris and co-workers who used a surface-functionalized colloidal silica template as a scaffold for the self-assembly of similarly surface-functionalized CdSe nanocrystals within the interstitials of the template.[39] The macroporous quantum dot solid was composed of a continuous network of 4 nm sized nanocrystals, which could be transformed, through short annealing at 650 °C, into a polycrystalline macroporous semiconductor with a RI contrast close to around 2.86.

4.2.2. Gas phase deposition. Though being experimentally more demanding, gas phase deposition schemes have become powerful tools for the fabrication of IOs where wet impregnation protocols fail owing to a lack of suitable (*i.e.* liquid or dissolved) precursors. Also, gas phase deposition oftentimes is the method of choice when it comes to materials processing requiring compatibility with protocols used in state-of-the-art microelectronic technologies. The two most widely used gas phase deposition methods involve i) chemical vapour deposition (CVD), including plasma-enhanced CVD and metal–organic CVD (MOCVD), and ii) atomic layer deposition (ALD). Such deposition schemes, requiring suitable mixtures of reactive gaseous precursors that are injected at reduced pressure into temperature-adjusted reactors, allow for a high level of precision and layer-by-layer deposition of uniform shell coatings around the microspheres. Therefore, gas phase deposition can in principle be a much more controlled process than solution phase impregnation, as nucleation and growth can be more finely adjusted and effects such as surface tension, wettability and diffusion are less of an issue or easier to control.

Published on 02 November 2012.

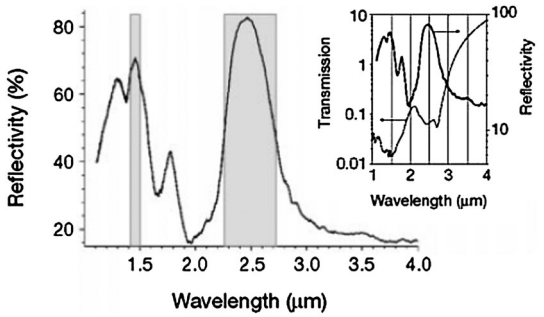

Fig. 12 Reflection and transmission spectra of a Si-IO. Shaded regions correspond to the predicted positions of the full photonic band gap around 1.46 μm and the pseudo gap at 2.5 μm. Reprinted by permission from Macmillan Publishers Ltd: *Nature*, 2000, **405**, 437, copyright 2000.[52]

From a materials point of view, the most important IO structure grown by CVD has clearly been that of silicon, the high RI (3.45) hallmark material of today's microelectronics industry. The first prototype Si IO has been tailored so as to place its band gap well above its absorption edge, thereby allowing coherent localization of light in a technologically important frequency range, namely, at telecommunication wavelengths around 1.5 μm.[52,53] To this end, a two-step, modified Stöber process was first employed to obtain monodisperse silica spheres with sizes variable between 600 and 1000 μm. Silicon was then grown inside the template by CVD using disilane (Si_2H_6) gas at 200 torr as a precursor and temperatures between 250 °C and 350 °C to adjust the filling fractions. Annealing of the composite at 600 °C was done to enhance crystallization and Si diffusion within the porous scaffold, and the template was selectively removed by fluoride-based etching. The close match between the experimental spectra and theoretical calculations suggested a full PBG centred at λ = 1.46 μm with a 5% gap to mid-gap ratio, and at the same time is testament to the excellent structural quality of the IO (Fig. 12 and 13, top). A similar CVD procedure based on digermane (Ge_2H_6) was adopted for the fabrication of a germanium IO, featuring an even higher dielectric constant than Si (ε = 16 for Ge *vs.* 12 for Si), yet still being transparent in the near IR (λ > 1850 nm) close to its full PBG at around 2 μm.[54]

A beautiful example demonstrating the versatility of CVD for IO fabrication was presented by Zakhidov *et al.* in 1998 (Fig. 13, middle). Along with a glassy carbon IO obtained *via* impregnation of a silica template with phenolic resin and subsequent HF etching of the template, CVD was used to synthesize highly opalescent and conductive (10 S cm^{-1}) graphite IOs with structural perfection down to the 10 nm scale.[55] A 1 : 3 molar ratio of propylene and N_2 was used as the feed gas, the reaction being maintained at 1 atm. pressure for 6 hours at 800 °C, followed by template removal with aqueous HF. Interestingly, the carbon modification can be adjusted by appropriately changing the synthesis conditions:

Diamond IOs are obtained by a seeding process based on 2 to 5 nm sized diamond seeds used as nuclei for further diamond growth. The seeds were deposited in the silica template along with carbon produced by plasma-enhanced

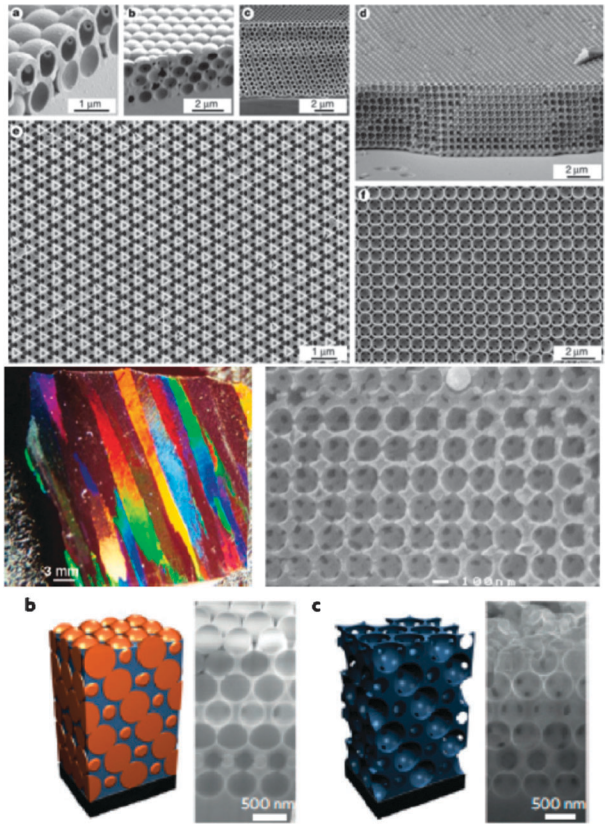

Fig. 13 Top: SEM micrographs of an on-chip grown silicon inverse opal. Adapted by permission from Macmillan Publishers Ltd: *Nature*, 2001, **414**, 289, copyright 2001.[53] Middle: Inverse opal of graphite produced by the CVD process using (A) 300 nm and (B) 200 nm silica templates. From *Science*, 1998, **282**, 897. Reprinted with permission from AAAS.[55] Bottom: Opal infiltrated with epitaxially grown GaAs (left) and inverted structure after template removal. Adapted by permission from Macmillan Publishers Ltd: *Nature Mater.* 2011, **10**, 676, copyright 2011.[47]

CVD using hydrogen and methane as feed stock. After HF etching of the template, a gradient-type structure was revealed composed of various forms of carbon, the topmost layers being cubic diamond: A micron thick external layer of diamond was coherently intergrown with the top part of the photonic structure consisting of a 20 to 30 μm thick cubic diamond IO. The underlying layer (300–500 μm) consisted of a mechanically soft carbon with a high sp^2-C fraction, while at the very bottom of the structure a 200 μm layer of a thin-walled cubic graphite IO was formed.[55]

Whereas IOs deposited by CVD are mostly polycrystalline structures with random crystallite orientation within the walls, deposition can be taken to an even higher level of perfection by making it, ultimately, epitaxial. Monolithic, ''single crystalline'' semiconductor IOs perfectly qualify as high-performance optoelectronic materials, as they reduce charge recombination and other loss processes and ensure high charge carrier mobilities and long carrier lifetimes. A first, yet decisive step towards this goal has recently been made by Braun and co-workers, who designed an elegant way to epitaxially grow an IO based on the direct gap III–V semiconductor GaAs, using

Published on 02 November 2012.

 This journal is © The Royal Society of Chemistry 2013

selective area epitaxy through a 3D opal template (Fig. 13, bottom).[47] By fine-tuning the growth of metal–organic precursors through a delicately patterned 3D mask under well-defined MOCVD conditions, homogeneous nucleation of the vapour species arsine and trimethylgallium in and around the template was achieved, resulting in the bottom-up growth of single-crystalline GaAs confined by the template. The architecture was refined by incorporating a 15 nm InGaAs layer sandwiched between n- and p-doped GaAs cladding layers, thereby producing a complex light-emitting heterostructure within a 3D IO. As a proof-of-concept, emission from the 3D PC-LED was demonstrated and tuned by solvent infiltration of the heterostructure, such that a coupling between the photonic and photoluminescence properties became feasible, thus modifying the light output.

Compared to CVD procedures, atomic layer deposition (ALD) is an excellent means to *conformally* deposit the material of choice into the porous template owing to its self-limited surface growth characteristics, while retaining the topology of the scaffold. ALD allows for a wide range of dielectrics, semiconductors and metals to be deposited at low temperatures, and the smoothness of the conformal layers is unparalleled owing to the layer-by-layer growth process. IOs fabricated by ALD span a wide range of materials, including Mn-doped ZnS, TiO_2, Ta_3N_5, and GaP.[56] ALD is a particularly promising tool for integrating higher levels of complexity into the IO structure, for example multilayer IOs created by backfilling an IO replica of the initial structure with additional layers of material, thereby reducing the air-sphere radius leading to non-close packed IO structures with strongly altered photonic properties.

4.2.3. Electrodeposition. The final method used for IO formation relies on the gradual nucleation and growth of a material within the interstitials by potentiostatic or galvanostatic deposition from solution. By this means, IOs have been obtained for materials that are challenging to deposit otherwise where sophisticated and expensive facilities are needed, such as for CdSe, CdS and Ge.[57] However, the scope of materials used for electrodeposition in opal templates has been modest so far. An advantage of this method is the high volume in-filling, yielding highly dense (and therefore high-RI) and rigid structures that are not prone to shrinkage upon template removal. Another advantage lies in the completeness of the process even when bulk colloidal templates, rather than thin films, are used: The growth front starts right at the bottom of the template and moves all the way through to the top of the opal template, rendering this process suitable to completely fill even topologically complex structures. The seminal example of electrodeposition of an IO has been presented by Wiltzius and Braun in 1999.[57]

CdSe and CdS were grown in an electrochemical cell in the potentiostatic mode with a PS template deposited on an ITO covered glass plate as working electrode, while using $CdSO_4$/SeO_2/H_2SO_4 or aqueous $CdCl_2$/$Na_2S_2O_3$ as electrolytes, respectively (Fig. 14). The versatility of this method lies in its simplicity – by choosing different starting materials, electrolytes and solvents, not only the growth kinetics and morphology of the walls can be fine-tuned, but also the thickness of the films can

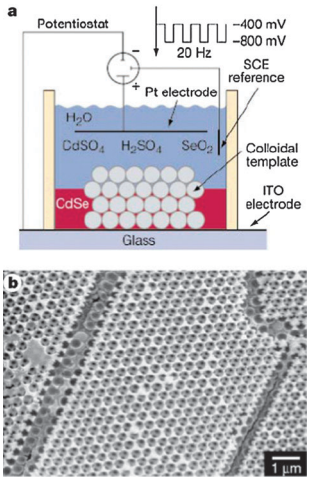

Fig. 14 Electrodeposition of CdSe into an opal template. Top: Experimental set-up, bottom: SEM image of a CdSe inverse opal grown in the voids of a PS template deposited on the ITO electrode Reprinted by permission from Macmillan Publishers Ltd: *Nature*, 1999, **402**, 603, copyright 1999.[57]

be controlled by tuning the charge passed through the sample during deposition. Finally, template directed electrodeposition should, and in part has already been demonstrated to be amenable to the deposition of a range of materials in a straightforward manner, including metals such as Au, as well as II–VI, III–V, and group IV semiconductors.

4.3. 2D photonic crystals

While 3D PCs are the ''all-rounders'' in photonic crystal technology and the architectures of choice when it comes to complete photonic band gaps, their little brothers – 2D PCs – may often be sufficiently versatile for applications not requiring omnidirectional photonic properties and at the same time be amenable to existing planar fabrication techniques. Moreover, coupling of the in-plane photonic modes to continuum modes and confinement of light within the 2D periodic architecture in the third dimension by index guiding adds to the usefulness of 2D PCs as ''quasi 3D PCs''.

From a materials point of view, much of what was discussed above for 3D PCs can be neatly transferred to 2D PCs, although much less effort has been put into exploring different fabrication and materials options in conjunction with 2D PCs as compared to their 3D counterparts. Various lithographic top-down strategies have yielded tailor-made photonic crystal slabs, however bottom-up self-assembled 2D PCs with demonstrated photonic features have been emerging only sluggishly over the past view years.

In the following, we will briefly highlight representative self-assembly protocols allowing the fabrication of 2D PC architectures. Although the assembly of nanoscale objects into 2D arrays on various length scales has developed into a burgeoning field since the early days of nanoscience, we will focus our attention on *periodic self-assembled* structures having *relevant length scales* for photonic applications, *i.e.* typically corresponding to visible and near IR wavelengths.

Published on 02 November 2012.

Published on 02 November 2012.

The self-assembly of 2D PCs basically draws on two techniques, the most prominent of which being the fabrication of opal monolayers by modified colloidal crystal assembly protocols and the inversion of such colloidal crystal monolayers (CCMs) into 2D monolayer inverse opals (MIOs). The second fabrication scheme relies on the microphase separation of specifically tailored block copolymers into planar 2D periodic arrays of polymers that can be suitably translated into hybrid or inorganic structures.

As discussed in 3.3, the template-directed deposition of CC films has been developed into a powerful tool to derive 3D IO structures however the deposition of exactly one monolayer of monodisperse colloidal spheres by capillary action and slow solvent evaporation puts an extra challenge on the deposition conditions. Nevertheless, rather simple protocols have been devised to tackle this goal, such as the interfacial synthesis of CCMs on planar substrates. In the air–liquid interface method, monodisperse colloidal particles, typically PS spheres in an ethanol–water suspension, are spread onto a water surface and spontaneously form close packed 2D arrays at the interface through attractive interactions between the particles. Controlled aggregation, ordering and consolidation of the monolayer may be facilitated by the addition of a spreading agent lowering the surface tension, such as dodecylsulfate.[58] Spreading of the particles is a consequence of the Gibbs–Marangoni effect describing the movement of a fluid due to a gradient in surface tension (induced by surfactant addition or using ethanol–water PS dispersions), resulting in mass transfer along the fluid–fluid interface away from the regions of low surface tension.

This basic procedure has been refined to obtain highly homogeneous, centimeter scale close-packed CCMs, for instance by applying a needle tip flow method designed by Asher and co-workers,[59] or by taking advantage of the facilitated arrangement of the particles by convective flow along a vortical water surface.[60]

The transfer of the as-obtained CCM onto a substrate is straightforward and can be done as follows: The substrate is immersed in the liquid before or after addition of the particle suspension, placed below the monolayer and lifted off while the CCM is deposited on the substrate surface (Fig. 15). Alternatively, the substrate is inserted into the water across the particle film and lifted up vertically at a steady speed as in Langmuir–Blodgett-type deposition, leaving colloidal arrays on both sides of the substrate.

This facile assembly and deposition scheme of CCMs can be extended further towards replicating these structures into inverse CCMs – MIOs – essentially the 2D counterparts of 3D IOs. By analogy with the replication strategies outlined in Section 4.2, a plethora of materials can be integrated into 2D inverse CCM architectures, boding well for the development of various inorganic, organic or hybrid photonic slabs, nets, and membranes.

To grasp the enormous potential for 2D IOM design enshrined in this fabrication procedure, the rapidly evolving field of nanosphere lithography would have to be reviewed. This type of "hybrid" lithography interfaces bottom-up and top-down deposition schemes by using self-assembled opal monolayers as masks through which large-scale nanoscale features can be deposited rather efficiently.

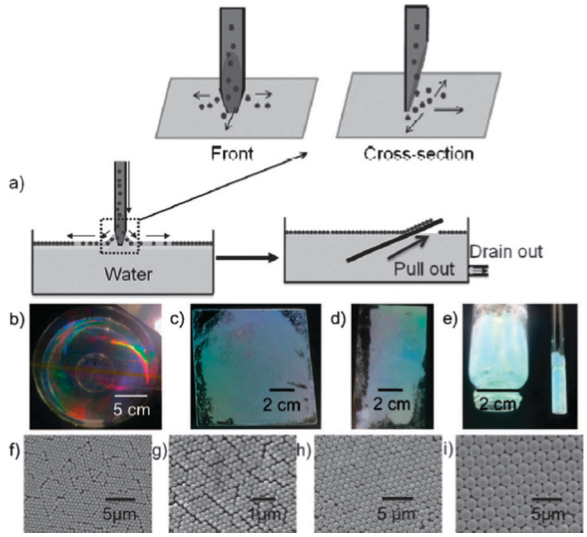

Fig. 15 (a) Fabrication of a 2D close-packed array of latex spheres by the needle tip flow method and transfer of the CCM onto a substrate by draining out the water or by lifting the assembly on a substrate. (b)–(i) Photographs and SEM images of various CCMs transferred onto different types of substrates. Adapted from ref. 59 with permission from John Wiley & Sons.

Different variations of this theme have been implemented to obtain a variety of metal-based as well as metal oxide, metal chalcogenide or polymer honeycomb lattices, including the deposition of metals by thermal evaporation, electron beam deposition or pulsed laser deposition, as well as solution-based methods, spin-coating and interfacial material deposition *via* reactions through freely floating CCM masks at the gas/liquid interface (Fig. 16).[61,62] The latter approach has been creatively used to fabricate a number of inorganic nanonets made of Ag_2S, PbS, $CaCO_3$ or Ag, having a pronounced photonic signature at optical wavelengths.

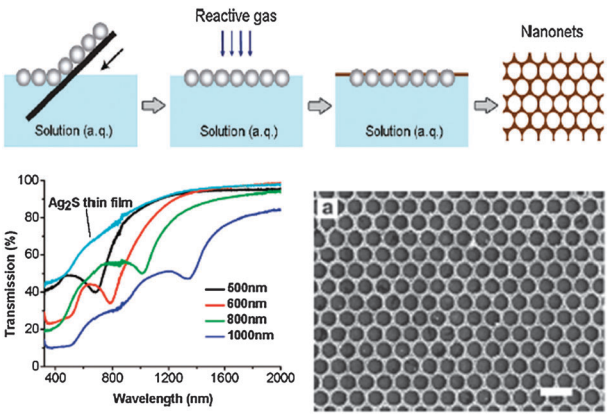

Fig. 16 Schematic of the fabrication of a free-standing nanonet obtained through nanosphere lithography at the liquid/air interface (top). Transmission spectra of Ag_2S nanonets showing guided mode resonances as compared to an unstructured Ag_2S film (bottom left) and SEM image of a Ag_2S nanonet obtained from 600 nm PS spheres (bottom right). Adapted with permission from *Chem. Mater.*, 2010, **22**, 476. Copyright 2010 American Chemical Society.[62]

This journal is © The Royal Society of Chemistry 2013

Published on 02 November 2012.

A materials class apt to self-assemble into 2D as well as 3D and 1D periodic structures directly without going through mask and etching steps, is the class of block copolymers (BPCs). Linear diblock copolymers consist of two chemically distinct polymer segments joined together at their endpoints, which tend to phase segregate into domains with sizes similar to the dimensions of the respective blocks (*i.e.* from a few nanometers up to about hundred nanometers).

Microphase separation induced by either cooling below the order–disorder transition or by solvent evaporation yields a variety of structures, including lamellar structures, body-centered cubic lattices composed of spheres, hexagonal-packed cylinders, or double gyroid cubic morphologies that exhibit photonic properties provided the domain size is large enough and defects are kept at a minimum. Domain sizes of about 400/n nm (n = refractive index of the material constituting the domain) have been obtained either by swelling one of the microphases with a homopolymer or other non-volatile additives.

The usually low RI contrast of the two microdomains impairing full band gaps and large bandwidths may be alleviated by selective loading of one domain with high index nanoparticles or by selective etching of one of the microdomains.[63] For example, a 2D PC has been obtained by Thomas and co-workers from roll-casting a high molecular weight polystyrene-*block*-polyisoprene copolymer, which microphase separates into cylindrical domains forming a regular hexagonal lattice. Owing to the intercylinder spacing of around 130–160 nm, the BCP film reflected blue light, albeit with a low bandwidth due to the small dielectric contrast between the microdomains.[64]

4.4. 1D photonic crystals

Having gone through the myriad embodiments of 3D and 2D photonic structures based on a variety of different materials, it becomes evident that there is a common underlying scheme for the self-assembly approaches in such systems: colloidal crystal assembly into 2D hexagonal close-packed monolayers or 3D cubic *fcc* lattices. The fabrication of 1D photonic structures puts yet another twist on the bottom-up assembly of periodic lattices, namely, directed (self-)assembly. 1D PCs – dubbed Bragg stacks, Bragg reflectors/mirrors or dielectric mirrors – are rarely "grown" by spontaneous, free energy driven self-assembly, although this is quite possible as seen for example in BCP-derived 1D PCs (see also chapter 4.3).[65] Rather, bottom-up processed periodic multilayer structures are assembled sequentially by spin-coating, dip-coating or layer-by-layer deposition schemes on a planar substrate. In such processes the directed assembly of nanoparticles, sol–gel precursors or polymer solutions onto a wettable substrate is driven by the action of centrifugal forces or capillary forces during solvent evaporation.

Although the deposition of multilayer structures is a multistep process often requiring drying and annealing steps between each subsequent layer, it does not require such intricate fabrication steps as colloidal crystal growth or template removal, thereby allowing for very robust and general fabrication schemes. However, an inherent shortcoming of most deposition schemes, especially spin- and dip-coating, is the lack of precise control over the layer thicknesses, which oftentimes vary by as much as 20% as a consequence of variations in solution concentration, aggregation/condensation state of the solution constituents, solvent evaporation or drying processes during fabrication of subsequent layers. This will give rise to deviations of the optical spectra from those for the ideal configuration, but may not severely deteriorate the desired functionality of the PC, *e.g.* with respect to sensing. In the following, we will highlight the most frequently adopted deposition schemes by presenting prominent and generic examples that can be generalized to other material systems.

4.4.1. Spin-coating. To date, spin-coating is the most general and widely applied method to prepare periodic multilayer stacks based on two different types of materials. As discussed in Section 3.3, large-area uniform films with thicknesses on the order of 10 nm to 500 nm can be deposited by the action of centripetal and, in some cases, capillary forces using myriad material and solvent combinations. 1D PCs that have been constructed in this way include purely polymer-based BSs used for instance as solvent or strain sensors, or hybrid BSs composed *e.g.* of the solvent-responsive polymer PMMA-*co*-PHEMA-*co*-PEGDMA and titania nanoparticle layers.[66] The bottom-up fabrication of hybrid organic–inorganic multilayer systems is generally challenging owing to the required stability of the soft material in the presence of the inorganic sol, which is deposited on top of the organic layer component. Since the solution containing the inorganic material is often strongly acidic as in the case of TiO_2 sols, spin-coating conditions need to be adjusted such that the chemical and morphological integrity of the sub-layer is retained.

A wide variety of inorganic material combinations has been integrated into 1D PCs by spin-coating protocols, including various transition and main group metal oxides,[67] zeolites,[68] clays,[69] metal–organic frameworks,[70] metals, and semiconductors. In the context of structurally robust all-inorganic architectures, different layer morphologies are of prime interest, especially when it comes to built-in, tunable porosity rendering such multilayer structures inherently functional. Besides the introduction of structural porosity by spin-coating surfactant-templated sols that are subsequently transformed into mesoporous metal oxide films with porosities up to 40%, the most widely applicable strategy for porosity tuning involves the deposition of nanoparticle suspensions to produce textural porosity of typically 10–35%, depending on the size of the nanoparticles and their packing density. This method excels by its universality, as it allows for the integration of various materials in nanoparticulate form, such as the prototype systems TiO_2 and SiO_2,[71] but also electronically conductive BSs built up from sputtered ITO and nanoparticle antimony-doped tin oxide,[72] or zinc oxide and iron oxide nanoparticle BSs.[73] The built-in textural porosity allows for an enhanced degree of environmental responsiveness, *e.g.* by refractive index tuning upon reversible or irreversible infiltration of the porous architecture with solvents, electrolytes,[74] dyes,[75] or polymers. Along these lines, distributed-feedback lasing of a vertical 1D nanoparticle TiO_2/SiO_2 PC resonance cavity infiltrated with the emitter poly(phenylenevinylene), PPV, has been demonstrated (Fig. 17).[76] Selective tunable color sensing has recently been

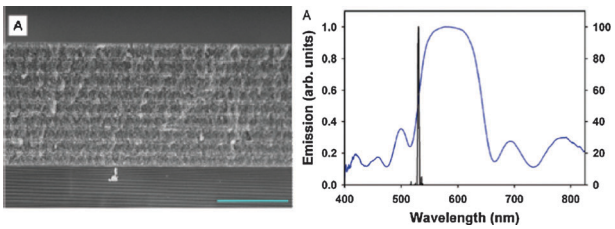

Fig. 17 Left: SEM image of an 11-bilayer SiO_2/TiO_2 nanoparticle-based Bragg stack (scale bar = 1 μm). Right: Reflectance spectrum of the BS infiltrated with PPV (blue) and emission spectrum of the composite above threshold (black). Adapted with permission from *Nano Lett.*, 2009, **9**, 4273. Copyright 2009 American Chemical Society.[76]

implemented by realizing both structural microporosity and textural mesoporosity in a single 1D PC platform by employing the nanoparticulate metal–organic framework ZIF-8 as active component. The size- and chemoselective adsorption of various alcohols in the structural pores of ZIF-8 gives rise to an optically encoded gas-detection capability of the BS, amplified by facile diffusion of the analyte and pore accessibility through the interstitial mesopores.[70]

Another elegant example of how interstitial porosity can be exploited was recently reported by Míguez and co-workers. TiO_2/SiO_2 nanoparticle BSs were used as ''hard template'' for infiltration with a polycarbonate solution.[77] This hybridization process imparts sufficient mechanical stability to the composite nanoparticle mold, which can subsequently be lifted off and transferred to arbitrary substrates without deterioration of the optical quality of the Bragg mirror (Fig. 18).

4.4.2. Dip-coating. Dip-coating of 1D PC multilayers can be viewed as a more specialized version of the spin-coating procedure, which has not yet been demonstrated for a large variety of materials due to the low amount of material transferred and its proneness to inhomogeneities. Therefore, it has unfolded its potential primarily in the realm of sol–gel-based oxides. In particular, this method has been pioneered by Míguez, Soler-Illia and co-workers for the fabrication of mesoporous metal oxides such as titania and silica with controlled structural nanoporosity introduced by structure-directing agents such as CTAB or Pluronics type poly(ethylene oxide)–poly(propylene oxide)-derived non-ionic surfactants like P123 or F127.[78] Dip-coating of metal oxide sols containing porogens typically requires a high degree of environmental control – ambient relative humidity in particular – to induce controlled evaporation induced self-assembly (EISA) at the organic–inorganic interface while the substrate is withdrawn vertically from solution. However, a delicate balance of factors like solution aging, solvent evaporation, substrate withdrawal speed and temperature is also a prerequisite for the achievement of highly ordered mesoporous films with controlled thickness. Dedicated aging, thermal stabilization treatments and template removal steps after deposition of each layer, renders dip-coating assembly of mesostructured materials a rather laborious and time-consuming procedure. Nevertheless, highly ordered multilayered films with porosity in excess of 40% could be produced by this technique, which present a versatile platform for modification of the pore surfaces by well-established silanization or other grafting protocols. Spatially resolved, selective integration of organic functions has been demonstrated for example by functionalizing the *meso*-TiO_2 layers with dihexadecyl phosphate, a molecule that can be selectively anchored to titania surfaces while leaving silica surfaces unmodified.[78]

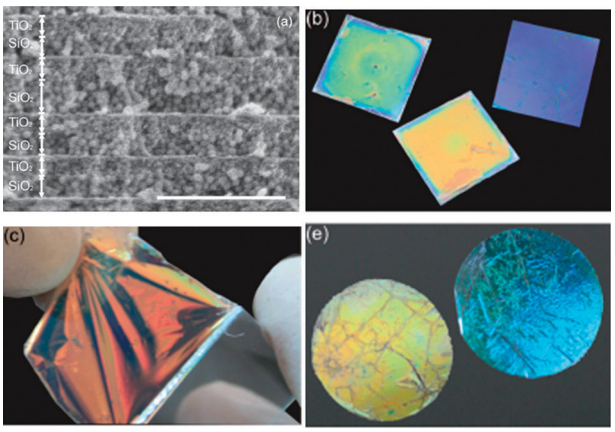

Fig. 18 Top left: cross-section SEM image of a nanoparticle-based BS infiltrated with poly(bisphenol-A-carbonate), scale bar 500 nm. Polymer-infiltrated BSs on substrates and flexible BSs peeled off the substrates (b–e). Adapted from ref. 77 with permission from Royal Society Publishing.

4.4.3. Layer-by-layer deposition. Layer-by-layer (LbL) assembly has become a powerful tool to deposit, from aqueous solutions, optical-quality conformal multilayer heterostructures with very low interfacial roughness, high compositional control and good stability, boding well for applications as antifogging, antifouling, antireflection or structural colour coatings. LbL electrostatic self-assembly involves the sequential deposition of polyelectrolytes onto planar or curved substrates and has materialized over the past 20 years in plentiful multilayer structures predominantly based on cationic and anionic organic polymers, but also inorganic polyelectrolytes such as clays and nanoparticles carrying a non-zero zeta potential and thus, surface charge. The first generation of optical-quality LbL structures with photonic properties surfaced from polyelectrolyte multilayers assembled from poly(acrylic acid) (PAA)/poly(allylamine hydrochloride) (PAH) and PAA/poly(sodium 4-styrenesulfonate) (SPS) layers showing alternating porous and dense regions induced by a reversible, pH-gated nanoporosity transition in the PAA/PAH layers.[79]

Subsequently, Cohen and co-workers demonstrated a photonic signature in TiO_2/SiO_2 nanoparticle-based systems assembled by polyelectrolyte-assisted LbL deposition, followed by calcination of the films to remove the polymer components.[80]

However, as compared to spin- and dip-coating protocols, fabrication of one high and low RI layer requires the deposition of about 20 nanoparticle/polymer bilayers owing to their small size of about 3–4 nm after calcination. As the layer assembly relies on sequentially immersing the substrates into the deposition and rinsing solutions, this process is rather time-consuming for hundreds of adsorbed layers and faster deposition schemes are required.

Published on 02 November 2012.

This journal is © The Royal Society of Chemistry 2013

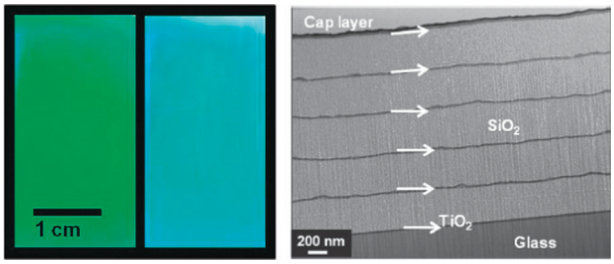

Fig. 19 Photograph at different angles of an 11-bilayer TiO_2/SiO_2 stack deposited on a microscope glass slide (left). Cross-sectional TEM image of a BS composed of alternating layers of TiO_2 (dark gray) and SiO_2 (light gray) nanoparticles assembled *via* spray LbL. Reprinted with permission from *Langmuir*, 2011, **27**, 7860. Copyright 2011 American Chemical Society.[81]

A possible alleviation to this problem other than using robotic coaters has recently been demonstrated by the automated spray-LbL assembly of polyelectrolyte-TiO_2 and -SiO_2 multilayer heterostructures including more than 800 individual deposition steps realized about 20 times faster compared to immersion LbL assembly.[81] By precisely controlling variables such as the spraying time, Bragg mirrors with reflectivities in excess of 90% were deposited on centimeter-large substrates with uniform optical quality (Fig. 19).

4.5. Defects in photonic crystals – perfecting imperfection

There is no such thing as a perfect crystal, be it an electronic crystal or photonic crystal in nature, and if it did exist what would it be good for? By this we mean that the functionality and utility of crystals usually originates from the properties of its defects. Yet every crystal has intrinsic and extrinsic defects, the former inherent in the lattice, the latter integrated into the lattice by design. Intrinsic defects or imperfections or disorder in crystals arise for example from vacancies, interstitials, stacking faults, dislocations, amorphous and crystalline domains as well as adventitious impurities built into the crystal lattice. They are often troublesome rather than useful and great efforts are made to reduce their population to improve for instance the electrical, optical, magnetic, thermal and mechanical properties of crystals. Extrinsic defects by contrast are introduced into the lattice intentionally to provide the crystal with purpose, which in the case of electronic crystals include doping, isomorphous substitution and non-stoichiometry.

Familiar outcomes of defects by design include control of charge, ion, proton and thermal transport, optical absorption and emission properties which can be orchestrated to create transistors, batteries, fuel cells, thermoelectric coolers, photocatalysts and light emitting diodes. These electronic defect states often exist in the forbidden electronic band gap and different types of defects create distinct functionality, which ultimately drives applications.

This discussion sets the stage for how to think about defects on passing from electronic to photonic crystals, the former fashioned at the scale of electron wavelengths, the latter at the light scale where intrinsic defects in photonic crystals still exist and cause difficulties such as transmission and emission light losses through multiple light scattering effects and strategies have been developed to minimize them. Extrinsic defects in photonic lattices, which create optical states within forbidden photonic band gaps, most commonly comprise point, line and planar structures fashioned at the scale of light, which through photon confinement enable the localization, guiding and transmission of light of use for making low threshold lasers, optical waveguides and filters.

The challenges faced in the field of self-assembled photonic crystals is how to incorporate extrinsic defects into the photonic lattice that perform at optical wavelengths, how to understand through theory, simulation and experimentation their optical and photonic properties, and how to efficiently couple light into and out of these structures to realize the aforementioned practical attributes to create a new generation of microphotonic devices. Impressive successes have been realized with making and understanding these kinds of defects but getting light in and out of these tiny defects to study and exploit their attributes remains fertile territory for future research.

A portfolio of approaches has been developed to introduce point, line and planar defects into different kinds of self-assembled photonic crystals, which include two-photon laser writing, laser micromachining, photolithography, electron beam lithography, spin-coating, layer-by-layer electrostatic self-assembly and micro-transfer printing.[82] While the experimental details for creating photonic crystal defects entirely by bottom-up methods or a creative integration of top-down and bottom-up approaches vary from one system to another, the end goal is always the same, namely control of the geometry, dimensions, location and precision to minimize light losses and maximize optical and photonic effects in both passive and active defects. Note that the former shows a static optical effect characteristic of the photonic defect while the latter responds dynamically to a particular chemical or physical stimulus.

In this context, the photonic crystals hosting the defect have usually been made of silicon, silica, organosilica, transition metal oxides and familiar polymers whereas the defects themselves, which are chosen to provide function (in parenthesis below) are more extensive and some prominent examples of the active ones include DNA (melting, chiral recognition) as illustrated in Fig. 20,[83] polypeptide (enzyme biodegradation kinetics), polyelectrolytes (swelling–shrinking solvent sensor), elastomers (mechanical switching), redox active polymers (electrochemical switching), fluorescent polymers, dyes and quantum dots (optical cavity), mesoporous titania (vapor sensing), clays (ion-exchange, anti-bacterial monitor) and zeolites (molecule recognition).[82]

5. Photonic crystals – ideas to innovation

5.1. A periodic table of bottom-up photonic crystals

An infinity of combinations of the elements of the periodic table has made accessible, through chemical synthesis, a palette of materials from which the canvas of materials applications in society has been painted. By understanding how structure and composition of materials relate to their properties

Published on 02 November 2012.

and how these properties connect to their functionality and performance, the ultimate goal of materials discovery can be achieved, namely utility.

This paradigm more or less describes the *modus operandi* of a chemical approach to the invention of new materials and their translation into a myriad of products and processes, and this approach has served humanity well for more than a century.

This is the story of materials in which the atomic constituents are close-packed leaving little room for anything else other than protons and lithium ions to enter the interstitial voids. However, early in the 20th century it was discovered that not all materials are dense, a revelation first realized with naturally occurring microporous zeolites that were thereafter synthesized in the laboratory. The aluminosilicate composition field of zeolites was soon expanded to include many other elements thereby propelling zeolites into mainstream solid state chemistry. Rapid developments in synthesis enabled the discovery of compositions that traversed the periodic table, that displayed insulating, semiconducting and metallic properties and with pore sizes that were gradually expanded over the years from microporous to mesoporous to eventually macroporous length scales, the latter being the subject of this tutorial review on photonic crystals.

As mentioned earlier, colloidal assembly of microspheres provided periodic macroporous materials, akin to naturally occurring opals, which could diffract light over all three spatial dimensions. The voids between the microspheres provided reaction chambers in which to perform host–guest inclusion chemistry that enabled replication of the opal in the form of its inverse, also able to diffract and to slow light. The voids in these inverse opals could themselves act as spaces in which to perform further host–guest chemistry or enable double inversion to recreate the original opal but with composition of choice.

With access to a periodic table of opal and inverse opal compositions, augmented by 1D porous Bragg mirrors and 2D porous membranes that joined the photonic crystal zoo, together with development of methods for controlling their morphology in a variety of forms, such as spheres, fibres, films and lithographic designs, the search began in earnest for applications of these light scale materials.

5.2. Photonic crystals – what are they good for?

Ultimately the test of any new material is its utility, what is it good for? In addressing this question for photonic crystals two main classes of materials have been investigated: (i) passive photonic crystals with the capacity to diffract, guide, localize, transmit and amplify light and (ii) active photonic crystals whose refractive index and/or dimensions and hence diffracted colour can be altered by chemical or physical stimuli.

As mentioned above, with access to a periodic table of compositions and a broad spectrum of chemical and physical materials properties, this has proven to be a fertile playground in which to mine for applications of photonic crystals.

5.3. Active photonic crystals

In the chemical arena active photonic crystal refractive index and/or dimensionally induced colour changes have been used

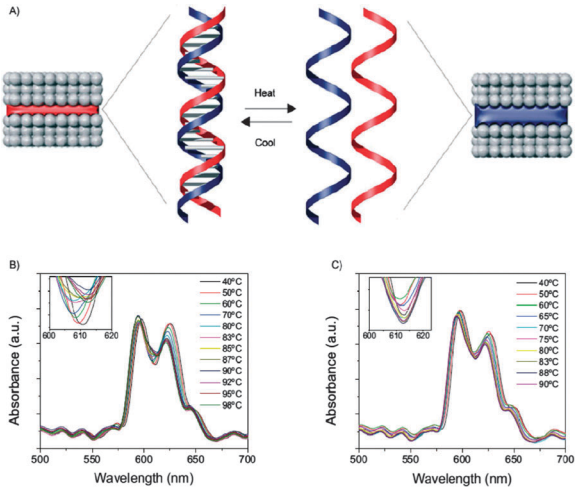

Fig. 20 Scheme illustrating the potential inherent to functional defects embedded in a 3D PC: (A) Optically encoded DNA denaturation and hybridization upon temperature treatment of a defect composed of DNA double strands. Transmission spectra of the DNA defect CC between 40 and 98 °C upon heating (B) and cooling (C). Adapted from ref. 83 with permission from John Wiley and Sons.

for label-free chemical and biochemical sensing, probing chiral recognition, monitoring DNA hybridization, watching enzyme activity, detecting bacteria and seeing silver anti-bacterial and chemical oscillators in action, checking food and water quality, viewing ion-exchange, enabling high resolution chromatographic separation, controlling surface wettability, and detecting heavy metals. In addition, slow photon amplification in photonic crystal materials has been shown to speed up the rates of photo-oxidation and photo-isomerization reactions relative to the same material devoid of the attributes of the photonic lattice.

The ability to tune the structural colour of photonic crystals through physically induced changes in their refractive indices and/or dimensions has been achieved through electrical, magnetic, optical, electro-optical, thermal and mechanical stimuli enabling demonstrations of full colour displays, colour tuneable photonic paper and ink, colour fingerprinting, thermal printing, colour coded battery state-of-charge, user-interactive bank note, credit card and passport anti-counterfeit systems and optical switching.

5.4. Passive photonic crystals

Passive versions of bottom-up photonic crystals have been explored for silicon and dye sensitized solar cells to improve their light trapping efficacy and performance, light emitting diodes to enhance their light extraction efficiency, dye and polymer lasers to improve their stability, versatility and performance, colourful coatings and formulations for a variety of purposes such as mobile phone and computer packaging, military camouflage, heat management in buildings, fabrics, cosmetics, paints and sunscreens.

Besides exploitation of their unique optical properties as outlined above, bottom-up photonic crystals have also been put to good use as macroporous high surface area supports, for example as a transparent conducting oxide electrode for housing electroluminescent and photoactive materials in displays and

Published on 02 November 2012.

This journal is © The Royal Society of Chemistry 2013

solar cells, as a gold–titania electrode for sensing hydrogen peroxide in the electrocatalysis of horseradish peroxidase, as a platinum electrode for the electro-oxidation of methanol, and as silicon, carbon and sulphur based electrodes for enhanced performance lithium ion batteries and supercapacitors.

5.5. Challenges

It is apparent that while a promising near-term future exists for photonic crystals made by bottom-up self-assembly methods, a number of technological hurdles remain to be overcome before they can realise their full potential. Many of these perceived or real world applications will require optimization of their thermal, mechanical, chemical, electrochemical and photochemical stability as well as the capacity to scale the production of photonic materials, as powders, films and coatings with high structural and optical quality, to industrial proportions in order to enable the cost-effective manufacture and commercialization of passive and active photonic crystal products.

In this context, encouraging recent developments at Merck, BASF, NanoPhotonics, Kent Displays, SRU Biosystems, Nanolab Solar and Opalux imply that a collection of bottom-up photonic crystal technologies could soon find their way to the market place for a myriad of colourful products. Such advances illuminate a bright future for the field!

6. Top-down or bottom-up: which way to go?

6.1. From the top

In the high-end top-down nanofabrication approach to high structural and optical quality photonic crystals used for controlling and manipulating the flow and colour of light, the market has been predicted to reach $34 Billion by 2016, fuelled mainly by applications in displays, optical fibres, light emitting diodes, discrete and integrated optical components, image sensors, solar cells, lasers and super-continuum sources, sensors and biosensors. Since 2009 the 46% compounded annual growth rate in these emerging photonic crystal technologies coupled with intense patent activity underway in the area is a clear indicator of the promising future for top-down photonic crystals in the market, www.companiesandmarkets.com.

Already in widespread use are one-dimensional photonic crystals found as coatings on lens and mirrors for controlling reflectivity as well as colloidal versions of one-dimensional photonic crystals dispersed in paints, to create bright iridescent coloration effects. Two-dimensional photonic crystals have been slower to find their way out of the research laboratory and are now beginning to find commercial applications in the format of photonic crystal fibres and thin film photonic crystals with their photonic lattice and associated photonic band gaps stretched out along the fibre axis and in the plane of the film, respectively. Two-dimensional photonic crystal fibres with, for example, a central air core enable the transmission of orders of magnitude higher optical power and information carrying capacity than conventional optical telecommunication glass fibres, while planar two-dimensional photonic crystals enable the construction of miniaturized optical cavities, lasers and sensors.

Perhaps of the greatest interest scientifically and technologically is the three-dimensional photonic crystal. With the right photonic lattice and made of the right material this three-dimensional photonic crystal construct has the unique property of providing an omnidimensional photonic band gap and the ability to control light over all three spatial dimensions. While the application opportunities for this "ultimate" photonic crystal are boundless, its greatest challenge for commercialization is to find a fabrication method that can master the stringent fabrication requirements demanded for 3D PCs with respect to structural and optical quality at sub-micron length scales, the capacity to incorporate point, line, bend and planar designer defects, the capability to couple light into and out of the photonic lattice, and the ability to scale devices from the very small, for integration of photonic crystal components into optical chips and optofluidic devices to the very large, for building photonic crystals into solar cells, light emitting diodes, lasers and sensors.

In this respect, the top-down nanofabrication technique dubbed direct laser writing (DLW) that uses two-photon laser patterning of diverse composition photoresists and is being commercialized in Karlsruhe, Germany, by Nanoscribe GmbH (www.nanoscribe.de), an interesting company to watch in terms of providing DLW instrumentation, a range of photoresists and one would imagine photonic crystal products in the future.

The overriding demand for successful commercialization of all kinds of photonic crystal optical components, whatever their dimensionality and scale, is manufacturability with control over intrinsic defects, which if not achieved lead to unacceptable light losses and deleterious effects on most envisioned optical applications.

6.2. From the bottom

This is where bottom-up assembled photonic crystals presented in this tutorial article come into the science, technology and commercialization story. It is considered unlikely that they will ever compete with top-down nanofabricated photonic crystals for high-end optical applications because of their lower degree of structural and optical quality and difficulty of controlling different kinds of intrinsic defects that creep into the synthesis procedures. Their strengths compared to top-down photonic crystals are however manifold and it is recognition and exploitation of these attributes that is facilitating development of a number of bottom-up photonic crystal technologies and commercialization opportunities.

These strengths include the ability to scale opal based photonic crystal films on both rigid and flexible substrates to industrially significant proportions (Fig. 21),[84] the choice of a periodic table of chemical compositions and materials properties for the photonic lattice, and the tolerance to defects for products that derive their functionality and utility from either passive or active structural colour.

So what does the future hold for the science and technology of bottom-up photonic crystals? The theory underpinning the optical properties of photonic crystals can be said to be mature and certainly sufficiently advanced to handle most scientific questions concerning synthetic photonic crystals whatever their

Published on 02 November 2012.

dimensionality. When it comes to photonic materials chemistry there is still much to explore aimed at developing new structure, property and function relations and how these provide new scientific and technological opportunities.

In this context one can envisage exciting developments with up-converting photonic crystals which employ slow photons to amplify the quantum yield for conversion of near infrared to visible light for enhanced efficiency light harvesting in solar cells. One can imagine how the unprecedented and selective adsorption capacity of metal and carbon based organic frameworks, nanoporous polymers and nanoporous molecular solids for H_2, CH_4 and CO_2 can be usefully exploited as a colorimetric sensor and pressure monitor for these gases when fashioned as a photonic crystal. One can see great opportunities for photonic crystal artificial leaves for converting $CO_2 + H_2O$ into solar fuels at globally significant conversion rates and efficiencies to ameliorate the climate, energy and population crisis, by taking advantage of slow photon amplified photocatalysis. Similarly, slow photon enhanced photonic crystal electrodes could achieve practical rates of photoelectrochemical H_2O splitting to H_2 for use as a clean fuel and as a reducing agent for converting CO_2 into hydrocarbons. One can picture molecular imprinted photonic crystals that can recognize pharmaceuticals through colour changes and find applications in drug storage and release as well as drug detoxification. One can foresee an electrochromic photonic crystal that enables the convolution of electrically tunable electronic crystal and photonic crystal effects into a single device providing thereby a distinctive means of creating and manipulating colour and greyscale in diverse kinds of colouration devices.

It should be clear from this photonic crystal ball gazing exercise that opportunities for creative fundamental and inventive applied research in the emerging field of bottom-up assembled photonic crystals is limited only by the fertility of one's imagination, one's ability to dream up photonic materials solutions to solve today's problems, and the courage and conviction to transition ones ideas to innovation, in order to monetize photonic crystals in the marketplace.

7. Conclusion

From this tutorial article it should be abundantly clear to the reader that since their discovery in the late nineties, photonic crystals made by bottom-up assembly methods are proving to be the 'classic overachievers'. They are shining very brightly in terms of the innovation content and scientific impact of the discoveries and inventions that have emerged on a daily basis which today shows no sign of waning and they are glowing intensely with respect to the myriad of promising opportunities that this knowledge has created for the development of diverse technology platforms that exploit the unique attributes of photonic crystals, from passive colour in cosmetics, sunscreens and paints to active colour in displays, security devices and sensors to enhanced light management systems in photochemistry and photocatalysis, light emitting diodes, solar cells and lasers. With access through chemistry to a periodic table of compositions, structures, surfaces and defects, chemical, physical and biological properties and a cornucopia of designer functions, we envision dazzling scientific and sparkling technological achievements for photonic crystals assembled from the bottom-up!

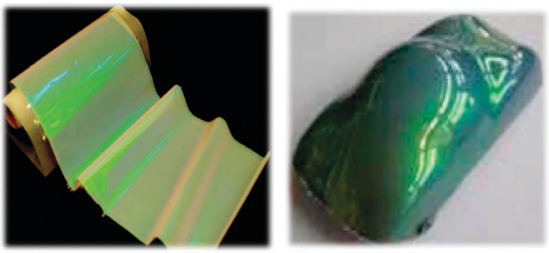

Fig. 21 Flexible opal film (left) and opal film moulded over a miniature car (right). Adapted from ref. 84 with permission of The Optical Society and www.Opalux.com.

Acknowledgements

G.v.F acknowledges support from the research centre OPTIMAS. VK acknowledges the Government of Ontario (ERA) and NSERC. B.V.L. acknowledges financial support by the cluster of excellence "Nanosystems Inititative Munich" (NIM), the Fonds der Chemischen Industrie and the Center for NanoScience (CeNS). GAO is Government of Canada Research Chair in Materials Chemistry and Nanochemistry and Distinguished University Professor at the University of Toronto, Toronto, Canada. GAO thanks the Natural Sciences and Engineering Research Council of Canada NSERC for strong and sustained support of his group's research. We thank Dr Wendong Wang for his creative art-science graphical representation of the "photonic crystal ball" theme of this tutorial article. None of this work would have been possible without the creative and insightful contributions of many colleagues and co-workers named in the bibliography of this article, who have helped make photonic crystal materials chemistry, materials science and technology in our research groups so exciting over the years.

Notes and references

1 S. M. Doucet and M. G. Meadows, *J. R. Soc., Interface*, 2009, **6**, S115.
2 E. Yablonovitch, *Phys. Rev. Lett.*, 1987, **58**, 2059.

Published on 02 November 2012.

 This journal is © The Royal Society of Chemistry 2013

Published on 02 November 2012.

3 S. John, *Phys. Rev. Lett.*, 1987, **58**, 2486.
4 P. Lodahl, A. F. van Driel, I. S. Nikolaev, A. Irman, K. Overgaag, D. Vanmaekelbergh and W. L. Vos, *Nature*, 2004, **430**, 654.
5 X. Hu, Q. Zhang, Y. Liu, B. Cheng and D. Zhang, *Appl. Phys. Lett.*, 2003, **83**, 2518.
6 C. Becker, S. Linden, G. von Freymann, M. Wegener, N. Tétreault, V. Kitaev and G. A. Ozin, *Appl. Phys. Lett.*, 2005, **87**, 091111.
7 P. P. Markowicz, H. Tiryaki, H. Pudavar, P. N. Prasad, N. N. Lepeshkin and R. W. Boyd, *Phys. Rev. Lett.*, 2004, **92**, 083903.
8 J. Martorell, R. Vilaseca and R. Corbalán, *Phys. Rev. A: At., Mol., Opt. Phys.*, 1997, **55**, 4520.
9 G. von Freymann, S. John, V. Kitaev and G. A. Ozin, *Adv. Mater.*, 2005, **17**, 1273.
10 V. Kitaev and G. A. Ozin, *Adv. Mater.*, 2003, **15**, 75.
11 J. I. L. Chen, G. von Freymann, S. Y. Choi, V. Kitaev and G. A. Ozin, *J. Mater. Chem.*, 2008, **18**, 369.
12 H. Zhang, X. Yu and P. V. Braun, *Nat. Nanotechnol.*, 2011, **6**, 277.
13 J. S. Sakamoto and B. Dunn, *J. Mater. Chem.*, 2002, **12**, 2859.
14 U. Kamp, V. Kitaev, G. von Freymann, G. A. Ozin and S. A. Mabury, *Adv. Mater.*, 2005, **17**, 438.
15 J. D. Joannopoulos, S. G. Johnson, J. N. Winn and R. D. Meade, *"Photonic Crystals: Molding the Flow of Light"*, Princeton University Press, 2008.
16 S. G. Johnson and J. D. Joannopoulos, *Opt. Express*, 2001, **8**, 173.
17 R. Hoffmann, *Solids and surfaces: a chemist's view of bonding in extended surfaces*, VCH Weinheim, New York, 1988.
18 S. A. Rinne, F. Garcia-Santamaria and P. V. Braun, *Nat. Photonics*, 2008, **2**, 52.
19 G. A. Ozin, K. Hou, B. V. Lotsch, L. Cademartiri, D. P. Puzzo, F. Scotognella, A. Ghadimi and J. Thomson, *Mater. Today*, 2009, **12**, 12 (and references therein).
20 K. J. M. Bishop, C. E. Wilmer, S. Soh and B. A. Grzybowski, *Small*, 2009, **5**, 1600.
21 D. A. Walker, B. Kowalczyk, M. O. de la Cruz and B. A. Grzybowski, *Nanoscale*, 2011, **3**, 1316.
22 F. Li, D. P. Josephson and A. Stein, *Angew. Chem., Int. Ed.*, 2011, **50**, 360.
23 S. Sacanna and D. J. Pine, *Curr. Opin. Colloid Interface Sci.*, 2011, **16**, 105.
24 M. L. Mastronardi, F. Maier-Flaig, D. Faulkner, E. J. Henderson, K. Kübel, U. Lemmer and G. A. Ozin, *Nano Lett.*, 2012, **12**, 337.
25 L. Cademartiri and V. Kitaev, *Nanoscale*, 2011, **3**, 3435.
26 V. Kitaev, *J. Mater. Chem.*, 2008, **18**, 4745.
27 N. Cathcart and V. Kitaev, *ACS Nano*, 2011, **5**, 7411.
28 B. A. Grzybowski, C. E. Wilmer, J. Kim, K. P. Brownie and K. J. M. Bishop, *Soft Matter*, 2009, **5**, 1110.
29 G. M. Whitesides and B. A. Grzybowski, *Science*, 2002, **295**, 2418.
30 J. H Moon and S. Yang, *Chem. Rev.*, 2010, **110**, 547.
31 S. Wong, V. Kitaev and G. A. Ozin, *J. Am. Chem. Soc.*, 2003, **125**, 15589.
32 J. Ge and Y. Yin, *Angew. Chem., Int. Ed.*, 2011, **50**, 1492.
33 D. C. Prieve, P. J. Sides and C. L. Wirth, *Curr. Opin. Colloid Interface Sci.*, 2010, **15**, 160.
34 J. Ge, L. He, Y. Hub and Y. Yin, *Nanoscale*, 2011, **3**, 177.
35 E. Vekris, V. Kitaev, D. D. Perovic, J. S. Aitchison and G. A. Ozin, *Adv. Mater.*, 2008, **20**, 1110.
36 B. Hatton, L. Mishchenko, S. Davis, K. H. Sandhagec and J. Aizenberg, *Proc. Natl. Acad. Sci. U. S. A.*, 2010, **107**, 10354.
37 K. Busch and S. John, *Phys. Rev. E: Stat. Phys., Plasmas, Fluids, Relat. Interdiscip. Top.*, 1998, **58**, 3896.
38 H. S. Sözüer and J. W. Haust, *Phys. Rev. B: Condens. Matter Mater. Phys.*, 1992, **45**, 13962.
39 D. J. Norris and Y. A. Vlasov, *Adv. Mater.*, 2001, **13**, 371.
40 X. Yu, Y.-J. Lee, R. Furstenberg, J. O. White and P. V. Braun, *Adv. Mater.*, 2007, **19**, 1689.
41 A. Rugge, J. S. Becker, R. G. Gordon and S. H. Tolbert, *Nano Lett.*, 2003, **3**, 1293.
42 O. D. Velev, P. M. Tessier, A. M. Lenhoff and E. W. Kaler, *Nature*, 1999, **401**, 548.
43 P. N. Bartlett, J. J. Baumberg, P. R. Birkin, M. A. Ghanem and M. C. Netti, *Chem. Mater.*, 2002, **14**, 2199.
44 S. Fan, P. R. Villeneuve and J. D. Joannopoulos, *Phys. Rev. B: Condens. Matter Mater. Phys.*, 1996, **54**, 11245.
45 A. Moroz, *Phys. Rev. Lett.*, 1999, **83**, 5274.
46 W. Y. Zhang, X. Y. Lei, Z. L. Wang, D. G. Zheng, W. Y. Tam, C. T. Chan and P. Sheng, *Phys. Rev. Lett.*, 1999, **84**, 2853.
47 E. C. Nelson, N. L. Dias, K. P. Bassett, S. N. Dunham, V. Verma, M. Miyake, P. Wiltzius, J. A. Rogers, J. J. Coleman, X. Li and P. V. Braun, *Nat. Mater.*, 2011, **10**, 676.
48 S. O. Klimonsky, V. V. Abramova, A. S. Sinitskii and Y. D. Tretyakov, *Russ. Chem. Rev.*, 2011, **80**, 1191.
49 J. E. G. J. Wijnhoven and W. L. Vos, *Science*, 1998, **281**, 802.
50 M. E. Turner, T. J. Trentler and V. L. Colvin, *Adv. Mater.*, 2001, **13**, 180.
51 H. Yan, C. F. Blanford, B. T. Holland, W. H. Smyrl and A. Stein, *Chem. Mater.*, 2000, **12**, 1134.
52 A. Blanco, E. Chomski, S. Grabtchak, M. Ibisate, S. John, S. W. Leonard, C. Lopez, F. Meseguer, H. Miguez, J. P. Mondia, G. A. Ozin, O. Toader and H. M. van Driel, *Nature*, 2000, **405**, 437.
53 Y. A. Vlasov, X.-Z. Bo, J. C. Sturm and D. J. Norris, *Nature*, 2001, **414**, 289.
54 H. Míguez, E. Chomski, F. García-Santamaría, M. Ibisate, S. John, C. López, F. Meseguer, J. P. Mondia, G. A. Ozin, O. Toader and H. M. van Driel, *Adv. Mater.*, 2001, **13**, 1634.
55 A. A. Zakhidov, R. H. Baughman, Z. Iqbal, C. Cui, I. Khayrullin, S. O. Dantas, J. Marti and V. G. Ralchenko, *Science*, 1998, **282**, 897.
56 D. P. Gaillot and C. J. Summers, in *Atomic Layer Deposition of Nanostructured Materials*, ed. N. Pinna and M. Knez, 1st edn, Wiley-VCH, Weinheim, 2011.
57 P. V. Braun and P. Wiltzius, *Nature*, 1999, **402**, 603.
58 J. Rybczynski, U. Ebels and M. Giersig, *Colloids Surf., A*, 2003, **219**, 1.
59 J.-T. Zhang, L. Wang, D. N. Lamont, S. S. Velankar and S. A. Asher, *Angew. Chem., Int. Ed.*, 2012, **51**, 6117.

60 F. Pan, J. Zhang, C. Cai and T. Wang, *Langmuir*, 2006, **22**, 7101.
61 C. Li and B. V. Lotsch, *Chem. Commun.*, 2012, **48**, 6169.
62 C. Li, G. Hong and L. Qi, *Chem. Mater.*, 2010, **22**, 476.
63 C. Paquet and E. Kumacheva, *Mater. Today*, 2008, **11**, 48.
64 T. Deng, C. Chen, C. Honeker and E. L. Thomas, *Polymer*, 2003, **44**, 6549.
65 J. Yoon, W. Lee and E. L. Thomas, *MRS Bull.*, 2005, **30**, 721.
66 Z. Wang, J. Zhang, J. Li, J. Xie, Y. Li, S. Liang, Z. Tian, C. Li, Z. Wang, T. Wang, H. Zhang and B. Yang, *J. Mater. Chem.*, 2011, **21**, 1264.
67 L. D. Bonifacio, B. V. Lotsch, D. P. Puzzo, F. Scotognella and G. A. Ozin, *Adv. Mater.*, 2009, **21**, 1641.
68 B. V. Lotsch, F. Scotognella, K. Moeller, T. Bein and G. A. Ozin, *Proc. SPIE*, 2010, DOI: 10.1117/12.854703.
69 B. V. Lotsch, C. B. Knobbe and G. A. Ozin, *Small*, 2009, **5**, 1498.
70 F. M. Hinterholzinger, A. Ranft, J. M. Feckl, T. Bein and B. V. Lotsch, *J. Mater. Chem.*, 2012, **22**, 10356.
71 S. Colodrero, M. Ocana and H. Míguez, *Langmuir*, 2008, **24**, 4430.
72 D. P. Puzzo, M. G. Helander, P. G. O'Brien, Z. Wang, N. Soheilnia, N. Kherani, Z. Lu and G. A. Ozin, *Nano Lett.*, 2011, **11**, 1457.
73 E. Redel, P. Mirtchev, C. Huai, S. Petrov and G. A. Ozin, *ACS Nano*, 2011, **5**, 2861.
74 S. Colodrero, A. Forneli, C. López-López, L. Pellejà, H. Míguez and E. Palomares, *Adv. Funct. Mater.*, 2012, **22**, 1303.
75 F. Scotognella, D. P. Puzzo, A. Monguzzi, D. S. Wiersma, D. Maschke, R. Tubino and G. A. Ozin, *Small*, 2009, **5**, 2048.
76 D. P. Puzzo, F. Scotognella, M. Zavelani-Rossi, M. Sebastian, A. J. Lough, I. Manners, G. Lanzani, R. Tubino and G. A. Ozin, *Nano Lett.*, 2009, **9**, 4273.
77 M. E. Calvo, O. Sánchez Sobrado, G. Lozano and H. Míguez, *J. Mater. Chem.*, 2009, **19**, 3144.
78 M. Cecilia Fuertes, F. J. López-Alcaraz, M. C. Marchi, H. E. Troiani, V. Luca, H. Míguez and G. J. d. A. A. Soler-Illia, *Adv. Funct. Mater.*, 2007, **17**, 1247.
79 L. Zhai, A. J. Nolte, R. E. Cohen and M. F. Rubner, *Macromolecules*, 2004, **37**, 6113.
80 Z. Wu, D. Lee, M. F. Rubner and R. E. Cohen, *Small*, 2007, **3**, 1445.
81 G. M. Nogueira, D. Banerjee, R. E. Cohen and M. F. Rubner, *Langmuir*, 2011, **27**, 7860.
82 A. Arsenault, F. Fleischhaker, G. von Freymann, V. Kitaev, H. Miguez, A. Mihi, N. Tétreault, E. Vekris, I. Manners, S. Aitchison, D. Perovic and G. A. Ozin, *Adv. Mater.*, 2006, **18**, 2779.
83 F. Fleischhaker, A. C. Arsenault, F. C. Peiris, V. Kitaev, I. Manners, R. Zentel and G. A. Ozin, *Adv. Mater.*, 2006, **18**, 2387.
84 O. L. J. Pursiainen, J. J. Baumberg, H. Winkler, B. Viel, P. Spahn and T. Ruhl, *Opt. Express*, 2007, **15**, 9553.

Published on 02 November 2012.

 This journal is © The Royal Society of Chemistry 2013